UNIVERSITY OF CALIFORNIA

SANTA BARBARA

Novel Vehicular Trajectories for Collective Motion from Coupled Oscillator Steering Control

by

Margot Kimura

A thesis submitted in partial satisfaction of the
requirements for the degree of
Master of Science

in

Mechanical Engineering

Committee in charge:
Professor Jeffrey Moehlis, Chair
Professor Francesco Bullo
Professor Mustafa Khammash

September 2007

The Thesis of Margot Kimura is approved:

_____

Professor Francesco Bullo

_____

Professor Mustafa Khammash

_____

Professor Jeffrey Moehlis, Chair

September 2007

Novel Vehicular Trajectories for Collective Motion from Coupled

Oscillator Steering Control

Abstract

Novel Vehicular Trajectories for Collective Motion from Coupled Oscillator

Steering Control

by

Margot Kimura

We explore the possibilities provided by an extension of the model for vehicle motion coordination by Leonard, Paley, and Sepulchre - by utilizing a slightly modified coupling function, we find that one can achieve a multitude of exotic coordinated trajectories.

To explain the underlying mechanism, we begin with a general analysis of a system of three vehicles with all-to-all coupling, in terms of both the full phase (θ) system and the reduced phase (ψ) system. The reduced system, subject to the Poincare-Bendixson Theorem, can only have two types of solutions: fixed points and periodic orbits. Simulation shows that the exotic trajectories we find are a result of periodic orbits in the reduced phase controller.

We then analyze the reduced phase controller with a particular coupling function that gives rise to such trajectories and provide approximate solutions, supported by simulation. We also build intuition on how solutions from the reduced controller are related to vehicular motion. We show that a multitude of exotic trajectories exist for this particular coupling function, and relate parameter values to the different

patterns.

Finally, we catalog the other possible types of coupling topologies for three vehicles, and repeat the above analysis for a different topology, which we have nicknamed the Arbiter coupling topology. We demonstrate in an extension of the previous example that one can find similar interesting vehicular trajectories for topologies other than all-to-all, and show that these trajectories can be found in a system of four vehicles under the Arbiter coupling topology.

To Euan,

with love

Contents

List of Figures

List of Tables

Acknowledgments

I wish to acknowledge and thank my advisor, Professor Jeffrey Moehlis, for his encouragement and guidance throughout my studies. I am lucky to have such an open and supportive advisor. I would also like to thank my committee members, Professor Francesco Bullo and Professor Mustafa Khammash, for their time in reading this thesis, as well as their insights and advice.

Thank you to the Hawaii Community Foundation, especially the Marion Maccarrell Scott and William James & Dorothy Bading Lanquist Scholarship Funds, for their continual support of my education.

Finally, I would like to thank my boyfriend, my family, and my friends, for their love and support.

Chapter 1

Introduction

The notion of using results from the coupled oscillator literature to control the motion of a group of vehicles is relatively new, and of interest because it is simple yet robust, and has been proven to work in a real-world system. To introduce this type of model, we will first begin with a brief background discussion while noting some relevant previous works in the separate subjects of coupled oscillator systems (Section 1.1), and the Dubins vehicle model (Section 1.2). We will then bring the two together in the following section, where we introduce the group motion coordination model by Leonard, Paley, and Sepulchre (Section 1.3), which will serve as the basis for our work. This will segue into our analysis of our variant of the Leonard, Paley, and Sepulchre (LPS) model, and the interesting vehicular trajectories we find.

1.1 Coupled Oscillator Systems

1.1.1 History

In 1665, the Norwegian mathematician Christiaan Huygens observed that the frequencies of two pendulum clocks suspended from the same beam slowly adjusted in time until they were identical, and the pendula phase-locked in anti-phase. This was the first documented observation of the synchronization of coupled oscillators. The two clocks were weakly coupled through the beam from which they both hung - the swinging motion of each pendulum was minutely transferred to the other pendulum via tiny movements in the beam. If the beam were perfectly rigid, the two clocks would have continued swinging at their natural frequencies, never synchronizing [16].

Since Huygens' first documentation of this phenomena, the same phase-locking behavior has been found in a multitude of natural and man-made systems composed of coupled oscillators. Given that an oscillator can be thought of as anything with sustained periodic behavior and that oscillators can phase-lock even if the coupling is very weak, it should not be surprising that phase-locked solutions can be found in such a wide range of dramatically different systems. A few examples of coupled oscillator systems include chirping crickets[1], an array of superconducting Josephson junctions, flashing fireflies, coupled electricity generators, pacemaker cells, and circadian rhythms [15, 16, 21]. A common result is synchronization,

---

[1]A cricket can be modeled as an oscillator in the following way: one can imagine the cricket's state as having a phase (angle), traveling around a circle, and every time the cricket's state passes zero phase, the cricket chirps.

where the oscillators phase-lock with the same phase.

1.1.2 Basic Models

Despite the fact that Huygens' observation was made so long ago, it was not until relatively recently that a significant amount of research has been directed towards studying the synchronization of coupled oscillators, perhaps due to the lack of a model to describe the behavior. In 1967, Winfree [23] created a mathematical model to describe how coupled oscillators evolve in time:

$$\dot{\theta}_i = \omega_i + \left(\sum_{j=1}^{N} X(\theta_j) \right) Z(\theta_i), \quad i = 1, ..., N.$$

Here, oscillator i has phase θ_i and natural frequency ω_i. The coupling between the oscillators is described by the functions X and Z: $X(\theta_j)$ shows the influence of each of the other oscillators on oscillator i, and $Z(\theta_i)$, the sensitivity function, determines the response of oscillator i [21, 23].

This model was further simplified and developed by Kuramoto [11, 21] in 1975, to the following equation for N coupled oscillators:

$$\dot{\theta}_i = \omega_i + \frac{K}{N} \sum_{j=1}^{N} \sin(\theta_j - \theta_i). \tag{1.1}$$

Like in the Winfree model, ω_i describes the natural (uncoupled) frequency of oscillator i and is drawn from a distribution, and the sum represents the total difference between phase of oscillator i and the phase of each of the other oscillators it is coupled to. The $\frac{1}{N}$ factor normalizes the sum. The constant K, called the coupling

3

strength, indicates how much of an effect the coupling has on each oscillator's phase at each instant in time.

Kuramoto also noticed that his model could be written in terms of an order parameter, which measures the net motion of the population. The complex order parameter is expressed as [11, 21]

$$r_{pc}e^{i\psi} = \frac{1}{N}\sum_{j=1}^{N}e^{i\theta_j}, \tag{1.2}$$

where $\psi \in [0, 2\pi)$ is the mean phase and $r_{pc} \in [0, 1]$ measures the phase coherence of the population. This can be manipulated and then substituted into Eqn (1.1) to yield

$$\dot{\theta}_i = \omega_i + Kr_{pc}\sin(\psi - \theta_i), \tag{1.3}$$

where $i = 1, \ldots, N$. This emphasizes that the primary influence on the phase of any particular oscillator is through the mean phase of the population, rather than the phase of each individual oscillator. This equation also provides an explanation for the mechanism underlying spontaneous synchronization: since the effective coupling strength of any solution is influenced by the coherence of the population, if a relatively large number of oscillators entrain to the synchronized state ($r_{pc} \approx 1$), they will in turn increase the strength of synchronization and recruit more oscillators to also synchronize. However, if the entrained oscillators have distributed phase ($r_{pc} \approx 0$), then the overall population will reach a level where the coupling will no longer have much influence, which explains why the distributed-phase so-

lution is less commonly found in natural systems. An excellent discussion of the history of these models as well as extensions can be found in [21].

Since Kuramoto's work appeared, research on coupled oscillator systems has exploded. The behavior of similar systems have been studied for a variety of different coupling functions and network architectures.

1.1.3 The Simplest System: N = 2

A significant amount of literature has focused on low-dimensional systems because they are more tractable to analyze than the general case. The simplest possible system is the case of $N = 2$ identical oscillators.

A general 2π-periodic coupling function f depending only on the phase difference of the two oscillators gives:

$$\dot{\theta}_1 = \omega + Kf(\theta_2 - \theta_1),$$
$$\dot{\theta}_2 = \omega + Kf(\theta_1 - \theta_2).$$

This system of equations can be simplified to a one-dimensional system: let $\psi = \theta_1 - \theta_2$. Then we have:

$$\dot{\psi} = K(f(-\psi) - f(\psi)).$$

Results from [4, 10, 12] show that the system has two persistent fixed points, which correspond to phase-locked solutions: $\psi = 0$ and $\psi = \pi$. The stability of all fixed points of the system can be shown to depend on the system parameters and

the form of the coupling function.

1.1.4 Low Dimensional Solutions: N = 3

Once one considers three oscillators, the dynamics of the system immediately become much richer. In both simulations and experiments for three coupled oscillators, attractors, bifurcations, cluster states, periodic orbits, tori, and heteroclinic cycles that may be robust have been found [2].

For the same class of coupling functions mentioned in the $N = 2$ case, the $N = 3$ system can be simplified to a two-dimensional system. This will be discussed in greater detail in the next section. The most important feature of the simplification is that the simplified subsystem provides a simple description of the types of solutions possible for the original system. Since the ψ system is two-dimensional, by the Poincare-Bendixson Theorem, we can be assured that there will not be any solutions more complicated than periodic orbits or fixed points in the ψ coordinates. Therefore, while we expect significantly more interesting results than in the $N = 2$ case, we can also expect that they will remain relatively tractable. For these reasons, we have focused our work on a system of three coupled oscillators.

1.1.5 More General Models

The transition from analyzing a system of three oscillators to four oscillators immediately introduces significantly more difficulty in finding solutions, since the Poincare-Bendixson Theorem is no longer valid for the ψ system.

In [8], Hansel, Mato & Meunier find heteroclinic orbits in systems of N coupled identical oscillators. The system they analyze is very similar to what we will examine in Section 2; specifically, the coupling function

$$\Gamma(x) = -\sin(x + \alpha) + r\sin(2x),$$

with various values of α. They also include the possibility of noise. Their results show the existence of two two-cluster states - in group theory terms, $(S_p \times S_{n_1-p}) \times (S_p \times S_{n_2-p})$ solutions - between which the system oscillates, before slowly converging to one of the two-cluster states. Here, n_i $(i = 1, 2)$ is the total number of oscillators in the ith two-cluster state, p is the largest cluster from each two-cluster state and satisfies $p < n_i$ for all i, and $n_1 + n_2 = N$. For the case of $N = 4$, the solution spends some time near one two-cluster state, then quickly shoots off to somewhere near the other two-cluster state, spends some time there, and then quickly returns to the vicinity of the first two-cluster state. This explains their strange result that the system is stable, in that it eventually settles to one of the two-cluster states, but that the linearization of each of the two-cluster states is unstable. However, they did not find these hetereoclinic connections for $N = 3$.

While there has been a fair amount of research on specific systems with large numbers of oscillators, a single approach that captures all possible solutions has not yet been completely formulated. However, there has been progress in providing solutions for generalized systems. We will specifically mention two approaches we have found.

The first approach focuses on symmetry arguments to show solutions for a class of networks. Specifically, the approach by Ashwin & Swift [4] assumes that the network is comprised of identical dissipative oscillators with weak coupling, and relies primarily on symmetry arguments to analyze networks with global coupling or either directed or bi-directional coupling in a ring. In this paper, they also investigate limit cycle solutions, structurally stable heteroclinic cycles, and degenerate behavior, where the oscillators decouple into subgroups [4].

The second approach focuses on the effect of network architecture on the results of coupled dynamical systems, or "cells". This very general approach, by Golubitsky & Stewart [20], as well as Leite and Dias (private communication), allows for different types of cells as well as different coupling laws between cells. By documenting the types of coupling, number of coupling links, and types of individual cells in the system, they have found a way to reduce a high-dimensional system to an equivalent lower-dimensional system which is much simpler to study. While some information is lost in simplifying the system and the preservation of the stability of solutions is not guaranteed, they have proven that solutions found for the low-dimensional analog exist in the original system. They have also shown that some results are due to the symmetry of a system, but that symmetry is not the only mechanism by which such solutions are possible [20].

1.2 Dubins' Vehicle

A widely studied motion control law for a single vehicle is given by the three-dimensional *Dubins system* [6, 22]:

$$\dot{x} = \cos(\theta)$$
$$\dot{y} = \sin(\theta) \qquad (1.4)$$
$$\dot{\theta} = u$$

subject to the constraint that

$$|u| \leq R. \qquad (1.5)$$

The minimum time problem for this system was originally proposed by Markov in 1889, and was analyzed in detail by Dubins in 1957 [6, 22]. Dubins found that a minimal time path necessarily exists for a particle traveling with constant unit speed along a continuously differentiable path in real Euclidean space from point u to point v with initial velocity vector U, terminal velocity vector V, and minimum radius of curvature R, if the path had an average curvature of less than or equal to R^{-1}. He named such a trajectory an *R-geodesic*. He proved that in the plane, an *R-geodesic* is necessarily a continuously differentiable curve consisting of not more than three pieces, each of which is either a straight line segment or an arc of a circle of radius R. Specifically, for a path consisting of straight lines (L), and circular arcs (C) of radius R, the optimal paths allowed are C, L, LC, CL, CC, CCC, and CLC, where the middle C arc in the CCC path has to be of length

$\geq \pi$. The above Dubins system has initial and terminal positions in (x, y), initial and terminal velocities in θ, and control variable u [6, 22]. This model for vehicle motion lends itself well to modeling realistic systems, such as cars and aircraft.

The Dubins system has been studied for a variety of properties. See [22] for a discussion and further analysis of the model.

1.3 Putting it All Together: The LPS Model

A number of schemes have been shown to be useful in the coordination of a group of vehicles, with each vehicle following a relatively simple control law. One scheme in particular takes advantage of existing results from the coupled oscillator community by using a Kuramoto-style equation to control the steering of N Dubins-style vehicles. Then, one can manipulate the stability of solutions in the phase model to provide coordinated group motions of the vehicles. We have based the majority of our work on studying a variant of this model by Leonard, Paley, and Sepulchre [13, 14, 15, 17, 18, 19], (similar to [9]), which will hereafter be referred to as the **LPS model**. For simplicity, their model assumes that the N Dubins-style vehicles are identical, move with constant unit speed, and are globally (all-to-all) coupled:

$$\dot{r}_n = e^{i\theta_n},$$
$$\dot{\theta}_n = u_n(r, \theta), \qquad n = 1, ..., N.$$
(1.6)

The complex vector r_n denotes the position of particle n, while the angle θ_n denotes

the orientation of its (unit) velocity vector. Since $r_n = x_n + iy_n$, with $(x_n, y_n) \in \mathbb{R}^2$, we will hereafter use the following equivalent equations for the position of each particle:

$$\dot{x}_n = \cos(\theta_n),$$
$$\dot{y}_n = \sin(\theta_n). \tag{1.7}$$

It can be shown that the above system is invariant to rigid group rotation and translation for controllers that are functions of only the relative positions and headings of the particles, defined as $r_{mn} = r_m - r_n$ and $\theta_{mn} = \theta_m - \theta_n$, respectively [13, 14, 15, 17, 18, 19]. The steering control of the vehicles u_n can be decomposed into the sum of three subcontrollers:

$$u_n = \omega_0 + u_n^{spac}(r, \theta) + u_n^{head}(\theta), \qquad n = 1, ...N, \quad \omega_0 \in \mathbb{R}. \tag{1.8}$$

The ω_0 term, typically a constant, determines whether the vehicles will move in straight lines ($\omega_0 = 0$) or circles ($\omega_0 \neq 0$), and the direction of rotation around the circle (given by the sign of $\omega_0 \neq 0$). The heading controller, u_n^{head}, depends only on the relative orientation of the vehicles and governs the overall motion of the group, while the spacing controller, u_n^{spac}, attracts the solutions to a given spatial formation to correct for random initial conditions. Given knowledge of the work done on coupled oscillators, it is intuitive to define the *phase controller* for the system as [15, 17, 19]:

$$\dot{\theta}_n = u_n^{phase} = \omega_0 + u_n^{head}(\theta). \tag{1.9}$$

11

A valid phase controller is given by a simplified version of the Kuramoto equation (1.1), in which all oscillators have the same natural frequency ω_0. This controller has been shown to generate trajectories that are either circular or linear, and in-phase, in anti-phase, or in a distribution of phases. Trajectories can also be classified in terms of the order parameter (1.2): synchronous solutions have order parameter with magnitude (equivalently, phase coherence) $r_{pc} = 1$, and balanced or incoherent solutions have order parameter with magnitude $r_{pc} = 0$. It is useful to note that the magnitude of the order parameter, r_{pc}, is equivalent to the speed of the center of mass, or the average linear momentum of the group [12, 13, 15, 17].

One can also recover a phase controller of the same form as the simplified Kuramoto model by designing the control with the gradient of a rotationally symmetric phase potential. Specifically, this gives

$$u_n^{phase} = \omega_0 + \frac{k}{N} \sum_{j=1}^{N} \sin(\theta_{mn}). \tag{1.10}$$

It has been found that for $k > 0$, the synchronized phase arrangements are the only asymptotically stable solution, whereas for $k < 0$, only the balanced solutions (satisfying order parameter $= 0$) are asymptotically stable [12, 13, 15, 17].

Constructing the spacing controller is more complicated in general, since it is designed to stabilize a specific formation. In [14, 15, 17, 18, 19], the derivation of a controller that stabilizes a circular formation and a proof of stabilization is given. The basic idea of the construction is to design a potential function which is minimum when the vehicles are in the desired configuration. Then, for $u_n^{head} = 0$,

it is possible to construct a Lyapunov function to demonstrate that the desired formation is asymptotically stable. For the overall system, one can use a composite Lyapunov function, made up of a linear combination of the Lyapunov functions used for the spacing and heading controls, to prove the stability of the overall desired configuration [13, 14, 15, 17, 18, 19].

The benefits of this style of model for controlling the motion of a group are clear: the model takes advantage of results from research on coupled oscillators and translates it into a simple but robust law governing individual vehicle motion that produces the desired overall group motion.

In the LPS model, vehicle behavior (i.e., motion in either circles or straight lines) is switched by changing the parameters ω_0 and k appropriately. A different switching scheme is presented for two vehicles in [10]. In this scheme, the system is tuned to a bistable state, and switching between stable solutions is induced by an input to one of the vehicles. Moreover, this scheme can be optimized to get switching for the lowest signal strength.

However, in both of these models, the coupling function is restricted to the first-mode sine term only. It may prove worthwhile to explore the effects of different coupling functions, such as including higher-mode terms, to see what other types of coordinated motion are possible. As shown in Section 1.1, coupled oscillator systems have been studied for coupling functions other than the basic sine of the phase differences. Using these slightly more complicated coupling functions in the LPS model, we have found that one can get trajectories that are much more exotic

than straight lines or circles, which may have advantages that will be discussed later. We will simplify our analysis by focusing on only the phase component of the vehicular motion, and by restricting the system to three vehicles. We will first analyze the properties of the general phase control, and then present a more detailed analysis of the resulting trajectories for a specific coupling function.

Chapter 2

Identical All-to-All Coupling:

Phase Dynamics

2.1   Equations and Symmetry

A system of three identical oscillators with all-to-all identical phase-difference coupling is given by

$$\dot{\theta}_n = \omega_0 + k \sum_{m \neq n} f(\theta_m - \theta_n), \qquad n = 1, 2, 3, \tag{2.1}$$

where $\theta_n \in [0, 2\pi)$ and the coupling function f is 2π-periodic. This system of equations is equivariant with respect to the group $S_3 \times T^1$, where S_3 is the six-element permutation group generated by

$$\sigma_1 : (\theta_1, \theta_2, \theta_3) \rightarrow (\theta_2, \theta_1, \theta_3),$$

$$\sigma_2 : (\theta_1, \theta_2, \theta_3) \rightarrow (\theta_2, \theta_3, \theta_1), \tag{2.2}$$

and T^1 is the circle group with action

$$\tau_\phi : (\theta_1, \theta_2, \theta_3) \rightarrow (\theta_1 + \phi, \theta_2 + \phi, \theta_3 + \phi) \tag{2.3}$$

for all $\phi \in [0, 2\pi)$. This means that if $(\theta_1(t), \theta_2(t), \theta_3(t))$ is a solution to Eqn (2.1), then, for any $\gamma \in S_3 \times T^1$, so is $\gamma \cdot (\theta_1(t), \theta_2(t), \theta_3(t))$.

As mentioned earlier, Eqn (2.1) can be reduced to a two-dimensional system by introducing the 2π-periodic variables $\psi_1 = \theta_1 - \theta_2$ and $\psi_2 = \theta_1 - \theta_3$:

$$\dot{\psi}_1 = \dot{\theta}_1 - \dot{\theta}_2 = k(f(-\psi_1) + f(-\psi_2) - f(\psi_1) - f(\psi_1 - \psi_2)),$$
$$\dot{\psi}_2 = \dot{\theta}_1 - \dot{\theta}_3 = k(f(-\psi_1) + f(-\psi_2) - f(\psi_2) - f(\psi_2 - \psi_1)). \tag{2.4}$$

Eqn (2.4) inherits equivariance with respect to the actions obtained from Eqns (2.2) and (2.3) on the ψ variables:

$$\hat{\sigma}_1 : (\psi_1, \psi_2) \rightarrow (-\psi_1, \psi_2 - \psi_1),$$
$$\hat{\sigma}_2 : (\psi_1, \psi_2) \rightarrow (\psi_2 - \psi_1, -\psi_1). \tag{2.5}$$

Note that $\hat{\tau}_\phi : (\psi_1, \psi_2) \rightarrow (\psi_1, \psi_2)$ acts as the identity for all ϕ. The actions $\hat{\sigma}_1$ and $\hat{\sigma}_2$ generate the permutation group S_3. We will sometimes find it convenient to think of ψ_1 and ψ_2 as being restricted to $[0, 2\pi)$, and other times it will be useful to allow them to take any real value.

2.2 Solutions and Bifurcations

Phase-locked solutions are characterized by each pair of θ variables always differing by a fixed value. Thus in the ψ variables, phase-locked solutions correspond

(a) S_3 Solution   (b) $S_2 \times S_1$ Solution   (c) Z_3 Solution
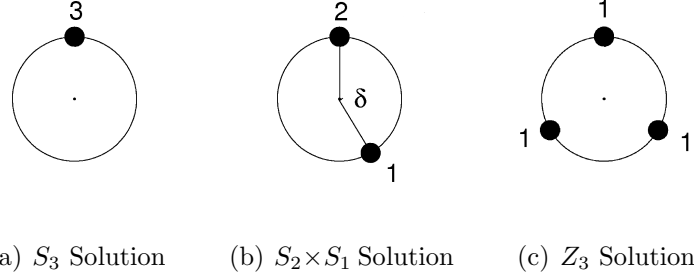
Figure 2.1: Phase locked solutions guaranteed to exist for any coupling function f. The locations of the dots on the phase circle are determined by the values of θ for the oscillators, with the number indicating how many oscillators share the same phase. These solutions are labeled according to their isotropy subgroup, as described in the text.

to fixed points. The existence, symmetry properties, stability properties, and possible bifurcations of phase-locked solutions are discussed below. As convenient, we will discuss these solutions in either the θ or the ψ variables. As we shall see, given a simple nondegeneracy condition, there are three types of phase-locked solutions that are guaranteed to exist for any coupling function f of the form in Eqn (2.1). The three solutions are the S_3, $S_2 \times S_1$, and Z_3 solutions, as shown in Figure 2.1. See [3, 4, 5] for alternative discussions.

2.2.1   The S_3 Solution: Fixed Point at $(\psi_1^*, \psi_2^*) = (0, 0)$

Proof of Existence

We prove the existence of a fixed point (ψ_1^*, ψ_2^*) for Eqn (2.4) by showing it satisfies $\dot{\psi}_1(\psi_1^*, \psi_2^*) = \dot{\psi}_2(\psi_1^*, \psi_2^*) = 0$. Substituting $(\psi_1^*, \psi_2^*) = (0, 0)$ gives

$$\dot{\psi}_1 = k(f(0) + f(0) - f(0) - f(0 - 0)) = 0,$$
$$\dot{\psi}_2 = k(f(0) + f(0) - f(0) - f(0 - 0)) = 0.$$

17

This holds for any function f, so $(0,0)$ always exists as a fixed point. Because ψ_1 and ψ_2 are 2π-periodic, this also implies the existence of fixed points at $(\psi_1^*, \psi_2^*) = (2\pi j, 2\pi m)$ for any integers j, m.

Symmetry

This phase-locked solution is invariant under the symmetry $S_3 = \langle \sigma_1, \sigma_2 \rangle$ in the θ variables, and $S_3 = \langle \hat{\sigma}_1, \hat{\sigma}_2 \rangle$ in the ψ variables, hence the name "S_3 solution". Since it corresponds to $\theta_1 = \theta_2 = \theta_3$, it is also sometimes referred to as the "in phase" or "synchronous" solution.

Stability Analysis

The Jacobian for Eqn (2.4) at the fixed point $(\psi_1^*, \psi_2^*) = (0,0)$ has a double eigenvalue $\lambda_{1,2} = -3kf'(0)$. Thus, the stability of the fixed point depends solely on the sign of the real part of $kf'(0)$: if $kf'(0)$ is positive (resp., negative), then the S_3 solution is stable (resp., unstable).

Bifurcations

Suppose that there is a bifurcation parameter which causes the shape of the coupling function f to change. It is immediately evident that the stability of the S_3 fixed point changes if the value $kf'(0)$ passes through zero as this parameter is varied. Because the fixed point at $(\psi_1^*, \psi_2^*) = (0,0)$ will persist for all f, this corresponds to an S_3-symmetric transcritical bifurcation.

Assuming that there are no fixed points on the invariant lines $\psi_1 = 0$, $\psi_2 = 0$,

18

or $\psi_1 = \psi_2$, for $(\psi_1, \psi_2) \in [0, 2\pi)$, at this bifurcation, a triangular heteroclinic connection appears between the fixed points at $(\psi_1^*, \psi_2^*) = (0, 0), (2\pi, 0)$, and $(0, 2\pi)$. Since these points are identified by the 2π-periodicity of ψ_1 and ψ_2, this can also be referred to as a homoclinic connection. Thus, [3] call this an $\mathbb{S}_3$ Transcritical/Homoclinic bifurcation, or $\mathbb{S}_{3\text{THB}}$. If the heteroclinic loop is attracting at the bifurcation, the system will have a stable limit cycle very close to the triangle on the side of the bifurcation where the S_3 solution is unstable. Such a bifurcation will occur in the example below.

2.2.2 The $S_2 \times S_1$ Solutions: Fixed Points at $(\psi_1^*, \psi_2^*) = (0, 2\pi - \delta)$, $(2\pi - \delta, 0)$, and (δ, δ) for $\delta \in (0, 2\pi)$

Proof of Existence for $(\psi_1^*, \psi_2^*) = (0, 2\pi - \delta)$

Evaluating Eqn (2.4) at $(\psi_1^*, \psi_2^*) = (0, 2\pi - \delta)$ and using the 2π-periodicity of f gives

$$
\begin{aligned}
\dot{\psi}_1 &= k(f(0) + f(-(-\delta)) - f(0) - f(0 - (-\delta))) \\
&= k(f(\delta) - f(\delta)) \\
&= 0, \\
\dot{\psi}_2 &= k(f(0) + f(\delta) - f(-\delta) - f(-\delta - 0)) \\
&= k(f(0) + f(\delta) - 2f(-\delta)).
\end{aligned}
$$

Thus, the $S_2 \times S_1$ solution is guaranteed to exist if there exists a δ^* that satisfies $f(0) + f(\delta^*) = 2f(-\delta^*)$. The following argument illustrates that for any coupling

function f satisfying the nondegeneracy condition $f'(0) \neq 0$, at least one such δ^* exists. First, define two new functions

$$c_1(\delta) = f(0) + f(\delta),$$
$$c_2(\delta) = 2f(-\delta).$$

(2.6)

The goal is to show that there exists a $\delta^* \in (0, 2\pi)$ satisfying $c_1(\delta^*) = c_2(\delta^*)$. By periodicity we know that $c_1(\delta + 2\pi) = c_1(\delta)$, and $c_2(\delta + 2\pi) = c_2(\delta)$. Letting $'$ denote derivation with respect to delta, or $\frac{d}{d\delta}$, we have that $c_1'(\delta) = f'(\delta)$ and $c_2'(\delta) = -2f'(-\delta)$. This implies that

$$c_1'(0) = f'(0) = f'(2\pi)$$
$$c_2'(0) = -2f'(0) = -2f'(2\pi).$$

(2.7)

Thus, $c_1(0) = c_2(0)$ but $c_1'(0) = -2c_2'(0)$. Moreover, the same relationships hold at 2π. Therefore, at some point between 0 and 2π, $c_1(\delta)$ and $c_2(\delta)$ must intersect, giving a viable value for δ^*. See Figure 2.2 for an illustration of this argument. While this argument guarantees that there is at least one δ^* satisfying this equality, it is possible to have more than one, corresponding to multiple phase-locked solutions with $\psi_1 = 0$. Note that the intersection $c_1(0) = c_2(0)$ does not provide a viable $S_2 \times S_1$ solution because this is the degenerate case of $\delta^* = 0$, which is the S_3 solution.

Similar arguments show that the symmetry-related fixed points $(\psi_1^*, \psi_2^*) = (2\pi - \delta, 0), (\delta, \delta)$ also exist for any coupling function f. Note that this implies the existence of fixed points at $(\psi_1^*, \psi_2^*) = (2\pi j, 2\pi m - \delta), (2\pi j - \delta, 2\pi m),$ and $(2\pi j + \delta, 2\pi m + \delta)$
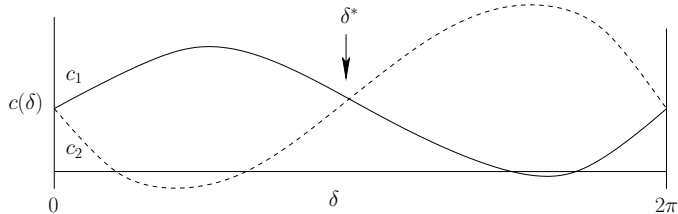
Figure 2.2: A cartoon of the functions $c_1(\delta)$ and $c_2(\delta)$ as defined in Eqn (2.6). Since the slopes of the functions have opposite signs at $\delta = 0$ (and at $\delta = 2\pi$), they must intersect at some point δ^*, which corresponds to the phase difference between the groups of oscillators for the $S_2 \times S_1$ solution.

for any integers j, m.

Symmetry

The phase-locked solution corresponding to $(\psi_1^*, \psi_2^*) = (0, 2\pi - \delta)$ is invariant under the group $S_2 = \langle \sigma_1 \rangle$ in the θ variables, and $S_2 = \langle \hat{\sigma}_1 \rangle$ in the ψ variables. Following [4], this is referred to as an $S_2 \times S_1$ solution; the S_2 corresponds to the permutation just mentioned, and the S_1 refers to the identity permutation acting on the other oscillator. The other phase-locked solutions are related to this one by symmetry, and are invariant under conjugate subgroups.

Stability Analysis

The Jacobian at the fixed point $(2\pi - \delta, 0)$ has eigenvalues $\lambda_1 = k[-f'(\delta) - 2f'(-\delta)]$ and $\lambda_2 = k[-2f'(0) - f'(\delta)]$. Note that the symmetry-related fixed points at $(2\pi - \delta, 0)$ and (δ, δ) have the same stability. These points have three possible stability types:

(1) if $k[f'(\delta) + 2f'(-\delta)] > 0$ and $k[2f'(0) + f'(\delta)] > 0$, the three fixed points are

21

sinks,

(2) if $k[f'(\delta) + 2f'(-\delta)] < 0$ and $k[2f'(0) + f'(\delta)] < 0$, the three fixed points are

sources, or

(3) if $k[f'(\delta) + 2f'(-\delta)] > 0$ and $k[2f'(0) + f'(\delta)] < 0$, or $k[f'(\delta) + 2f'(-\delta)] < 0$

and $k[2f'(0) + f'(\delta)] > 0$, the three fixed points are saddles.

Bifurcations

Bifurcations occur when either $f'(\delta) + 2f'(-\delta) = 0$ or $f'(\delta) + 2f'(0) = 0$.

Depending on the relative values of $f'(\delta)$, $f'(-\delta)$, and $f'(0)$ for different parameters

of f, the fixed points' stability can change to or from a sink, source, or saddle in

a pitchfork or saddle-node bifurcation, cf. [3]. Such solutions are involved in the

$\mathbb{S}_{3\text{THB}}$ bifurcation described above, and can also be involved in the related global

saddle-node heteroclinic bifurcation identified in [2].

2.2.3 The Z_3 Solutions: Fixed Points at $(\psi_1^*, \psi_2^*) = \left(\frac{2\pi}{3}, \frac{4\pi}{3}\right)$ and $\left(\frac{4\pi}{3}, \frac{2\pi}{3}\right)$

Proof of Existence for $(\psi_1^*, \psi_2^*) = \left(\frac{2\pi}{3}, \frac{4\pi}{3}\right)$

Evaluating Eqn (2.4) at $(\psi_1^*, \psi_2^*) = \left(\frac{2\pi}{3}, \frac{4\pi}{3}\right)$ and using 2π-periodicity of f gives

$$\dot{\psi}_1 = k(f(-\tfrac{2\pi}{3}) + f(-\tfrac{4\pi}{3}) - f(\tfrac{2\pi}{3}) - f(\tfrac{2\pi}{3} - \tfrac{4\pi}{3})),$$

$$= k(f(-\tfrac{2\pi}{3} + 2\pi) + f(-\tfrac{4\pi}{3} + 2\pi) - f(\tfrac{2\pi}{3}) - f(\tfrac{2\pi}{3} - \tfrac{4\pi}{3} + 2\pi))$$

$$= k(f(\tfrac{4\pi}{3}) + f(\tfrac{2\pi}{3}) - f(\tfrac{2\pi}{3}) - f(\tfrac{4\pi}{3}))$$

$$= 0,$$

$$\dot{\psi}_2 = k(f(-\tfrac{2\pi}{3}) + f(-\tfrac{4\pi}{3}) - f(\tfrac{4\pi}{3}) - f(\tfrac{4\pi}{3} - \tfrac{2\pi}{3}))$$

$$= k(f(-\tfrac{2\pi}{3} + 2\pi) + f(-\tfrac{4\pi}{3} + 2\pi) - f(\tfrac{4\pi}{3}) - f(\tfrac{4\pi}{3} - \tfrac{2\pi}{3}))$$

$$= k(f(\tfrac{4\pi}{3}) + f(\tfrac{2\pi}{3}) - f(\tfrac{4\pi}{3}) - f(\tfrac{2\pi}{3}))$$

$$= 0.$$

A similar argument shows that a fixed point exists at $(\psi_1^*, \psi_2^*) = (\tfrac{4\pi}{3}, \tfrac{2\pi}{3})$ for any coupling function f. Note that this implies the existence of fixed points at $(\psi_1^*, \psi_2^*) = (2\pi j + \tfrac{2\pi}{3}, 2\pi m + \tfrac{4\pi}{3})$, and $(2\pi j + \tfrac{4\pi}{3}, 2\pi m + \tfrac{2\pi}{3})$ for any integers j, m.

Symmetry

The fixed point $(\psi_1^*, \psi_2^*) = (\tfrac{2\pi}{3}, \tfrac{4\pi}{3})$ corresponds to a solution for which $\theta_1 = \theta_2 + \tfrac{2\pi}{3}$ and $\theta_2 = \theta_3 + \tfrac{2\pi}{3}$. This is typically called the "splay state" because θ_1, θ_2, and θ_3 are equally spaced around the unit circle. This solution is invariant under the three-element cyclic group Z_3 generated by

$$(\theta_1, \theta_2, \theta_3) \rightarrow \left(\theta_2 + \frac{2\pi}{3}, \theta_3 + \frac{2\pi}{3}, \theta_1 + \frac{2\pi}{3} \right), \tag{2.8}$$

hence the name "Z_3 solution". In terms of the ψ variables, this solution is invariant under $\langle \hat{\sigma}_2 \rangle$, which is isomorphic to the group Z_3.

The fixed point $(\psi_1^*, \psi_2^*) = (\frac{4\pi}{3}, \frac{2\pi}{3})$ is invariant under the group Z_3 generated by

$$(\theta_1, \theta_2, \theta_3) \rightarrow \left(\theta_3 + \frac{2\pi}{3}, \theta_1 + \frac{2\pi}{3}, \theta_2 + \frac{2\pi}{3} \right) \tag{2.9}$$

in the θ variables, and $\langle \hat{\sigma}_2 \hat{\sigma}_1 \rangle$ in the ψ variables.

Stability Analysis

The Jacobian at this fixed point $(\frac{2\pi}{3}, \frac{4\pi}{3})$ has eigenvalues $\lambda_{1,2} = k(-\frac{3}{2}(f'(\frac{2\pi}{3}) + f'(\frac{4\pi}{3})) \pm \frac{3i}{2}|f'(\frac{4\pi}{3}) - f'(\frac{2\pi}{3})|)$. Thus, unless $f'(\frac{4\pi}{3}) = f'(\frac{2\pi}{3})$, this fixed point will be either a spiral sink or a spiral source.

Bifurcations

At $f'(\frac{2\pi}{3}) + f'(\frac{4\pi}{3}) = 0$, the fixed point switches between a spiral sink and a spiral source, which is an indication of a Hopf bifurcation, as found in [3].

2.3   A Particular Example

As an example, we now consider the coupling function

$$f(\varphi) = \mu_1 \sin(\varphi) + \mu_2 \cos(\varphi) + \mu_3 \sin(2\varphi), \tag{2.10}$$

which will provide a spectrum of novel trajectories when applied to vehicle motion coordination using the LPS model. This coupling function is compared with a sinusoidal coupling function (as used in [15]) in Figure 2.3: our example coupling

24
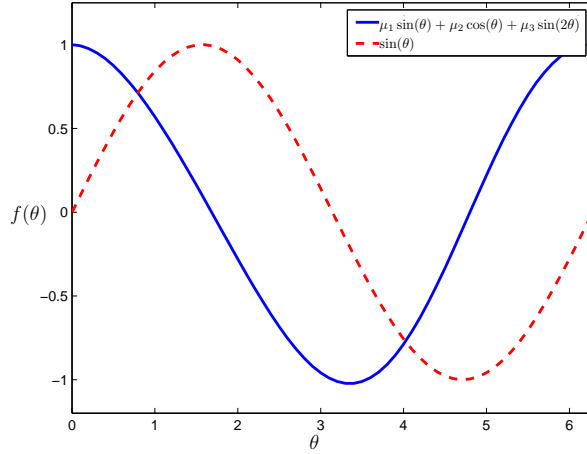
Figure 2.3: Comparison between the coupling function (2.10) with $\mu_1 = 0.1, \mu_2 = 1$, and $\mu_3 = -0.06$ and sinusoidal coupling function $f(\theta) = \sin(\theta)$.

function can be viewed as a perturbation of a phase shift of the sinusoidal coupling function. The above analysis predicts that both a $\mathbb{S}_{3\text{THB}}$ bifurcation involving the S_3 and $S_2 \times S_1$ solutions and, independently, a Hopf bifurcation involving the Z_3 solutions will occur at $\mu_1 + 2\mu_3 = 0$. Numerical bifurcation analysis shows that for $\mu_2 = 1, \mu_3 = -0.06, k = 1$ and when treating μ_1 as the bifurcation parameter, the Hopf bifurcation is subcritical, and that the branch of unstable periodic orbits turns around in a saddle-node bifurcation of periodic orbits to give stable periodic orbits; see Figure 2.4. This figure also shows that the phase space for the system can be divided into two triangles bounded by the invariant lines $\psi_1 = 0, \psi_1 = 2\pi, \psi_2 = 0, \psi_2 = 2\pi$, and $\psi_1 = \psi_2$. Trajectories in these triangles are related by symmetry, and the resulting vehicular trajectories are identical. Thus, without loss of generality, we will assume that all initial conditions are chosen such that the system moves in the lower right triangle.

25

In the following, we focus on parameter values $\mu_1 = 0.1$, $\mu_2 = 1$, and $\mu_3 = -0.06$, with phase space as shown in the panel (c) of Figure 2.4. Here almost all initial conditions will converge to either the stable limit cycle or the stable Z_3 solution at $\left(\frac{2\pi}{3}, \frac{4\pi}{3}\right)$.
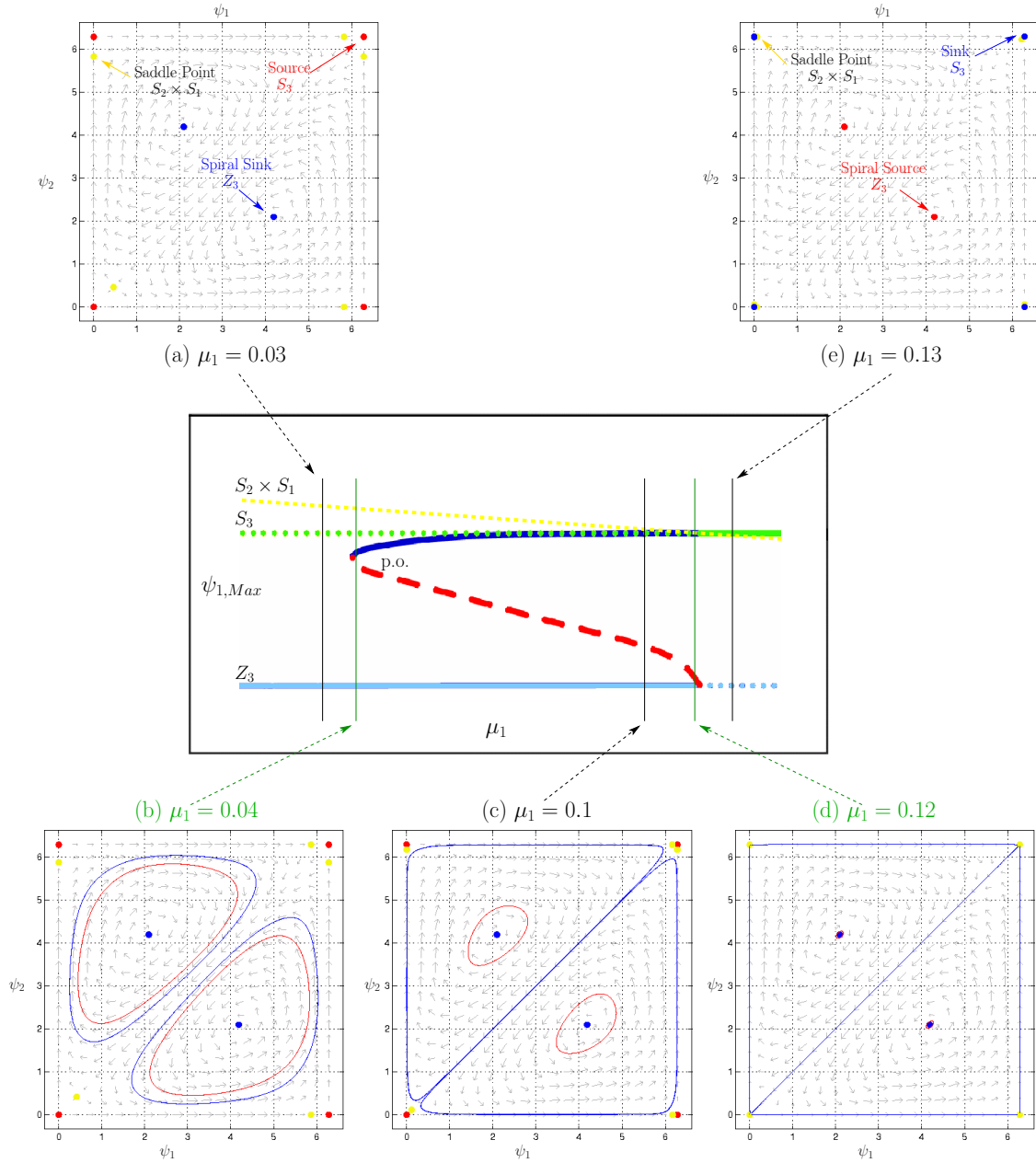
Figure 2.4: The bifurcation diagram in terms of μ_1, showing the phase portraits at several values of μ_1 of interest for $\mu_2 = 1$ and $\mu_3 = -0.06$. In the (ψ_1, ψ_2) plane, yellow dots represent saddle points, red shows sources or unstable periodic orbits, and blue represents sinks or stable periodic orbits. Solid (resp., dashed or dotted) lines in the bifurcation diagram indicate stable (resp., unstable solutions).

27

Chapter 3

Identical All-to-All Coupling:

Vehicular Trajectories

We now illustrate the richness of possible vehicular trajectories for Eqn (1.6) with identical all-to-all phase-difference steering control by considering the coupling function given in Eqn (2.10) with parameters $\mu_1 = 0.1$, $\mu_2 = 1$, and $\mu_3 = -0.06$, as for the above example. If the system converges to the stable Z_3 solution, then the vehicles will move either in circles or in straight lines, depending on the value of ω_0, with each instantaneously moving in a direction with an angle of $\frac{2\pi}{3}$ with respect to the others. Such motion has been found for the LPS model with the coupling function $f(\theta) = \sin(\theta)$ [13, 14, 15, 17, 18, 19]. However, if the system converges to the stable limit cycle, then the vehicles can display more exotic trajectories, as seen for example in Figure 3.1. For this reason, we will focus our analysis on the solutions that converge to the stable limit cycle.
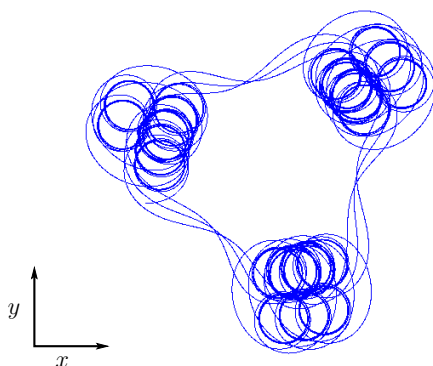
Figure 3.1: An example trajectory for v_1 with parameters $\mu_1 = 0.1, \mu_2 = 1, \mu_3 = -0.06, \omega_0 = k = 1$. This trajectory is taken over many cycles of the system in the (ψ_1, ψ_2) plane.

Motion along the limit cycle is not uniform: the system slows near each of the fixed points, and moves quickly in regions away from a fixed point. As will be explained in the following, it is from this non-uniform motion that the trajectories get their peculiar shapes. We first present an explanation of the vehicular motion in an intuitive way, then validate the intuition with results from numerical simulations. Without loss of generality, we will primarily restrict discussion to the motion of vehicle 1 (denoted v_1) only.

3.1   The Intuitive Description

We first divide the motion of the system in the (ψ_1, ψ_2) plane and the motion of v_1 into constituent parts. We will then relate the position of the system along the stable periodic orbit in the (ψ_1, ψ_2) plane to trajectories of the vehicles in the (x, y) plane to provide intuition on how these kinds of trajectories are formed.

The motion of the system can be naturally divided into six boxes along the limit

cycle, as seen in Figure 3.2. In the first, third, and fifth boxes, the system slowly passes near an $S_2 \times S_1$ fixed point. Starting from the lower-left corner and working counter-clockwise, we will call these boxes **A**, **B** and **C**. In the second, fourth, and sixth boxes, the system is leaving the vicinity of one fixed point and approaching another. Starting from the line $\psi_2 = 0$ and going counterclockwise, we will call these boxes **1**, **2** and **3**.

The overall vehicle motion in Figure 3.1 can be decomposed into identical units, each of which contains a cluster and a tail. We will name the tail connecting the units a **long excursion**. Each cluster can be further broken down to show two general types of behavior: small approximately circular orbits, which we will call **small orbits**, and the roughly semi-circular excursions that connect the small orbits, which we will refer to as **short excursions**. The vehicle path in a single unit can be described as a cycle through a small orbit followed by a short excursion to another small orbit, followed by a second short excursion to a third small orbit, followed by a long excursion to the next cluster. This is illustrated in Figure 3.2.

Simulations of the vehicles show that when the system in the (ψ_1, ψ_2) plane is in a lettered box (near a fixed point), the vehicles move in a small orbit, and when the system is in a numbered box, the vehicles undergo an excursion. This is expected, since the vehicles would move in a circle if the system were actually at the fixed point because, at a fixed point, generically, $\dot{\theta}_j = \text{constant} \neq 0$. Therefore, one can intuitively expect the vehicles to show a sort of switching behavior between small orbits and excursions as the system moves in the ψ plane.

| Boxes: $3 \to A \to 1$ | Boxes: $1 \to B$ | Boxes: $B \to 2$ | Boxes: $2 \to C \to 3$ |
| Transition in and out of a small orbit | Short excursion to another small orbit | Small orbit to another short excursion | Small orbit to long excursion |

Three units: one full circuit

Corresponding motion of the system in the (ψ_1, ψ_2) plane
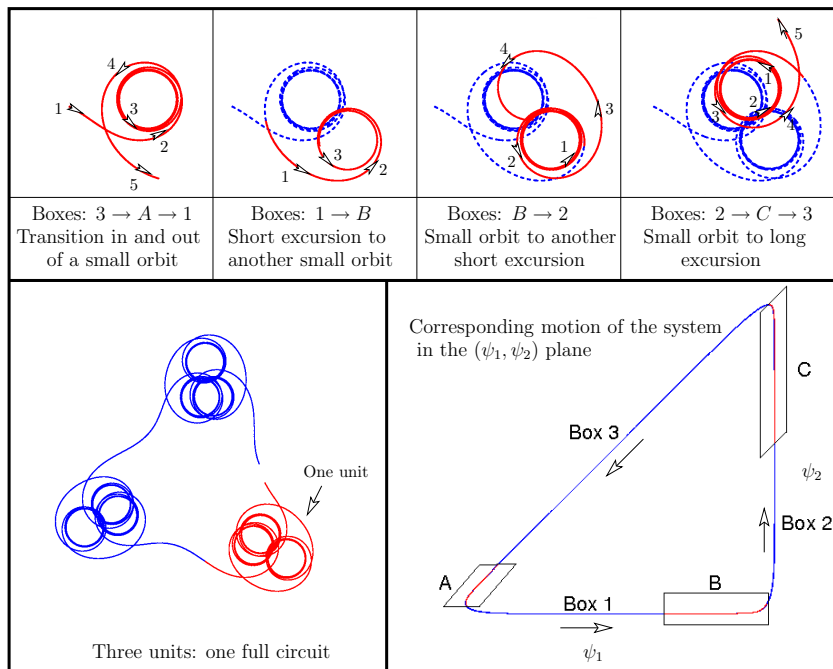
Figure 3.2: Behavior of v_1 in the (x, y) plane with corresponding position of the system in the (ψ_1, ψ_2) plane. The top explains the motion of v_1 within one unit: follow the ordered arrows in the time-series of pictures. The bottom-left panel shows one full circuit of vehicle motion and the bottom-right panel shows the various boxes in the (ψ_1, ψ_2) plane.

Box	ψ Behavior	θ Behavior	Vehicle Motion
1	$\psi_1 \uparrow$ to $\approx 2\pi$ $\psi_2 \approx 0$	θ_1 & $\theta_3 \uparrow$ at the same rate θ_2 temporarily $\downarrow$	v_1 & v_3: short exc v_2: long exc
2	$\psi_2 \uparrow$ to $\approx 2\pi$ $\psi_1 \approx 2\pi$	θ_1 & $\theta_2 \uparrow$ at the same rate θ_3 temporarily $\downarrow$	v_1 & v_2: short exc v_3: long exc
3	$\psi_1 \approx \psi_2 \downarrow$ together to ≈ 0	θ_2 & $\theta_3 \uparrow$ at the same rate θ_1 temporarily $\downarrow$	v_2 & v_3: short exc v_1: long exc

Table 3.1: Relative phase and resulting behavior of all 3 vehicles in terms of position in the (ψ_1, ψ_2) plane. Here, $\uparrow$ means "increase(s)", $\downarrow$ means "decrease(s)", and "exc" is short for "excursion(s)." The definition of "excursion" is given in the text.

Earlier, we restricted discussion to the motion of v_1 because the motion of v_2 and v_3 were identical to but out of phase with the motion of v_1. This alternating motion is summarized in Table 3.1.

3.2 Numerical Analysis and Validation

3.2.1 Box Definition

To validate the above intuition, we need to be more precise about the boundaries of the boxes. Since the vehicles are always moving in a smooth and roughly circular trajectory, it is natural to define the boxes in terms of the instantaneous radius of curvature of the vehicles' trajectories. This was calculated from simulation data for each point by finding the radius of the circle defined by that point and its two neighboring points. Using this for measuring the motion of v_1 gives the plot in Figure 3.3. The long excursion includes a segment where the radius of curvature passes through infinity. However, since we will use the radius of curvature as a measure for constructing the lettered boxes, which involves only the minima of
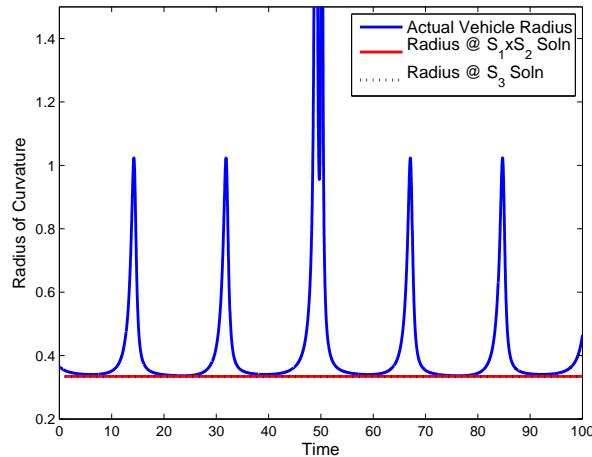
Figure 3.3: Measurements of the radius of curvature for v_1 moving in the trajectory shown in Figure 3.1 with the approximations at each nearby fixed point. It is evident from the periodic flat troughs that the radius of curvature of the vehicle's motion spends a significant amount of time at an approximately constant value. Moreover, the value of that constant value is very close to the radius of curvature the vehicles' motion would have if the system were at the $S_2 \times S_1$ fixed point.

Figure 3.3, it does not matter that the radius of curvature blows up during the long excursion. The lettered boxes were chosen by calculating where the radius of curvature for v_1 was within 0.01 of the minima of each trough, as seen in Figure 3.4. Boxes 1, 2, and 3 are then defined as the intervening lengths of the periodic orbit in the ψ plane.

3.2.2 Box Analysis: Approximate Solutions

Within each box, we present an approximate solution with a few simplifying assumptions.

Near a fixed point, the behavior of the system is approximately the same as if the system were actually *at* the fixed point. From this observation, we provide
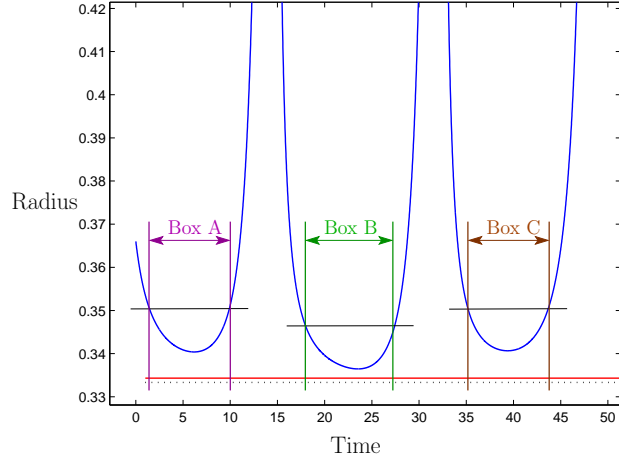
Figure 3.4: An enlargement of Figure 3.3, showing how close the actual instantaneous radius of curvature of v_1 comes to the approximated values, and how the radius of curvature defines the location of the lettered boxes. The dotted line represents what the radius of curvature would be at the S_3 solution, and the red solid line represents the radius at the $S_2 \times S_1$ solution. The line segments show where the radius of curvature of v_1 is within 0.01 of its minimum for each box. The edges of the boxes correspond to the intersections of these line segments with the radius of curvature of v_1. The numbered boxes are then assigned as the intervening spaces between lettered boxes.

an approximate solution for the behavior of the vehicles when the system is in one of the lettered boxes. At a fixed point, the coupling function becomes a constant. Plugging into our full system equations in θ, we have

$$\dot{\theta}_1 = \dot{\theta}_2 = \dot{\theta}_3 \equiv \varpi,$$

where ϖ is a constant. This is easily integrated, giving:

$$\theta_i(t) = \varpi t + \theta_{0i}.$$

This corresponds to the following equations in the (x, y) plane:

$$\dot{x}_i = \cos(\varpi t + \theta_{0i}),$$

$$\dot{y}_i = \sin(\varpi t + \theta_{0i}).$$

These equations can also be integrated, yielding

$$x_i = \frac{1}{\varpi} \sin(\varpi t + \theta_{0i}),$$

$$y_i = -\frac{1}{\varpi} \cos(\varpi t + \theta_{0i}),$$

corresponding to motion in a circle of radius $\frac{1}{\varpi}$.

For the particular coupling function discussed in the example above, $\varpi = \omega_0 + 2k\mu_2$. Plugging in the values for ω_0, k, and μ_2 used in the example, we find that the vehicles move in circles with radius $\frac{1}{3}$ if the system is at an S_3 solution. When the system is at one of the $S_2 \times S_1$ solutions, found for these parameters to be at $(0.11511, 0.11511)$, $(0, 2\pi - 0.11511)$, or $(2\pi - 0.11511, 0)$, the radius of the motion of v_1 is approximately 0.334317. From panel (c) of Figure 2.4 we see that the trajectory comes closer to the $S_2 \times S_1$ solutions than to the S_3 solutions. Thus, we expect the radius of the vehicular motion of v_1 in the lettered boxes to be closer to the radius predicted by having the system at the $S_2 \times S_1$ solution. As one can see in Figure 3.4, this approximation is very close to the results obtained from the actual simulation.

In the numbered boxes, we can approximate the behavior of the system by noting that in Box 1, $\psi_2 \approx 0$, in Box 2, $\psi_1 \approx 0$, and in Box 3, $\psi_1 \approx \psi_2$ and both decrease from a value close to 2π to a value close to 0 at about the same rate.

Taking $\psi_2 = 0$ (which is approximately true in Box 1) in Eqn (2.4), we obtain $\dot{\psi}_2 = 0$ and

$$\dot{\psi}_1 = \dot{\theta}_1 - \dot{\theta}_2 = k(f(-\psi_1) + f(0) - 2f(\psi_1)), \tag{3.1}$$

a one-dimensional differential equation. Similarly, taking $\psi_1 = 2\pi = 0$ (which is approximately true in Box 2) in (2.4) gives the same formula as (3.1) but with $\psi_1 \rightarrow \psi_2$.

Finally taking $\psi_1 = \psi_2 \equiv \psi$ (which is approximately true in Box 3), we obtain

$$\dot{\psi}_1 = \dot{\psi}_2 = \dot{\psi} = k(2f(-\psi) - f(0) - f(\psi)), \tag{3.2}$$

which is related to Eqn (3.1) through $\psi_1 \rightarrow -\psi$.

3.2.3 Validation

As shown in Figure 3.4, the trajectories of the vehicles while in the lettered boxes is quite close to the radius of curvature predicted by the approximate solutions. The lettered boxes were defined by noting where the radius of curvature of the motion of the vehicles was within 0.01 of the minimum radius from simulation data for the system. For reference, we also show the radius corresponding to the S_3 solution.

In the numbered boxes, we have found one-dimensional equations to approximate the dynamics of the system in Eqn (3.1). Numerical integration of the approximate solutions very closely match the data from simulation in all three boxes. The approximate solutions are nearly identical in Boxes 1 and 2, so only the simulation for Box 1 is shown. We have found that the one-dimensional approximation for the system's behavior is valid even in appropriate parts of the lettered boxes, as one might expect from the assumptions that generated the approximations and the graph of the (ψ_1, ψ_2) plane in Figure 3.2. The results of numerically integrating the behavior in Boxes 1 and 3 compared to simulation data for v_1 are shown in Figures
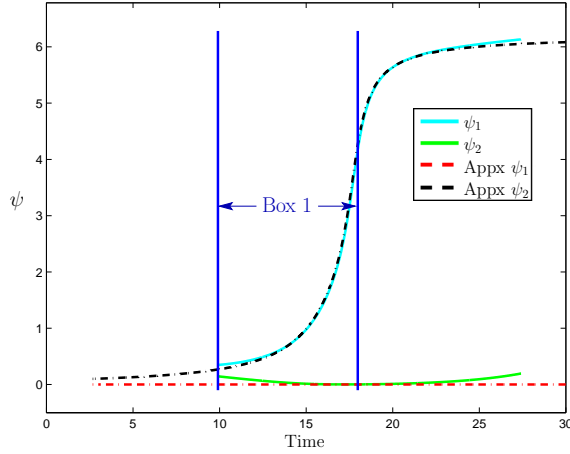
Figure 3.5: Demonstration of the validity of the approximation leading to Eqn (3.1): the graphs of the approximate solutions in Box 1 and actual simulation data show that the assumptions taken are reasonable.

3.5 and 3.6, respectively.

3.2.4 The Spirograph in the Kaleidoscope

The ω_0 and k terms effectively control the curvature of the individual trajectories and the speed at which the system moves through the ψ plane, respectively. It has been found in simulations that the shape of the vehicular trajectories, even in transients, depends only on the ratio $\frac{\omega_0}{k}$, and that changing either ω_0 or k independently will scale the pattern. This can be seen most easily in an equivalent form of Eqn (2.1):

$$\dot{\theta}_n = k \left(\frac{\omega_0}{k} + \sum_{m \neq n} f(\theta_m - \theta_n) \right), \qquad n = 1, 2, 3. \tag{3.3}$$

In this more explicit form, it is clear that the variable k just scales time, while the actual dynamics depend only on the constant $\frac{\omega_0}{k}$, which can be thought of as
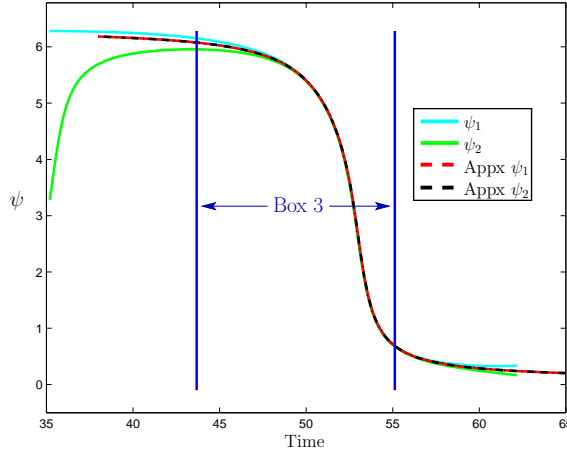
Figure 3.6: Demonstration of the validity of the approximation leading to Eqn (3.2): the graphs of the approximate solutions in Box 3 and actual simulation data show that the assumptions taken are reasonable.

the effective natural frequency. Since we have constrained our vehicles to have constant unit speed, the only way that the vehicles can compensate for a larger (resp., smaller) k (with appropriately scaled ω_0), which would make the vehicles move more quickly (resp., slowly), is to produce a smaller (resp., larger), scaled, version of the exact same pattern, even in transients. This behavior is demonstrated in Figure 3.7.

There are many possible trajectories found by varying the $\frac{\omega_0}{k}$ ratio, which have a base shape resembling a pattern from a Spirograph[1]. It is possible to obtain a regular overall trajectory (global) shape with any number of sides that either passes through the approximate center of the polygon, or travels exclusively along

---

[1]A "Spirograph" is a toy invented by Denys Fisher, and was first introduced to the United States in 1966 by Kenner, Inc. The name "Spirograph" is a trademark of Hasbro, Inc. The toy allows the user to create intricate designs: the user puts a pen on a point within a circle, which rotates around the inside or outside of another shape, typically also a circle. The geometric curves produced by a Spirograph are mathematically known as hypotrochoids and epitrochoids [1]. An interactive applet demonstrating what patterns are possible with a Spirograph can be found at [7].
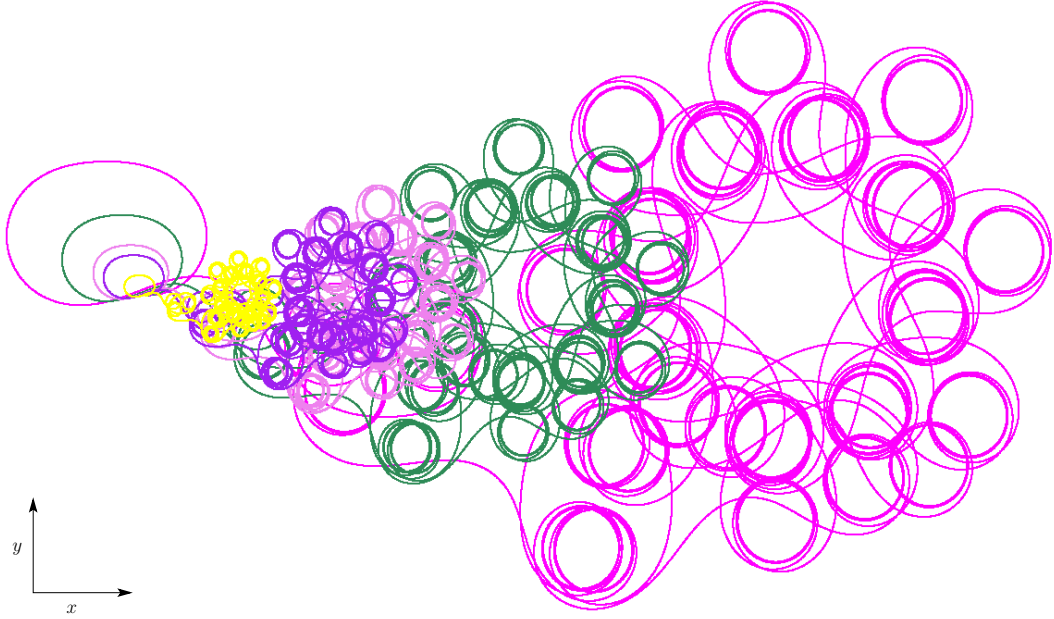
Figure 3.7: Five trajectories with the same initial conditions in (x, y) and (ψ_1, ψ_2), and with the same value for $\frac{\omega_0}{k}$, but with different values of k (and appropriately scaled ω_0).

the edges. In other words, the radius of the global shape can be made to be anywhere between zero and infinity. Moreover, as one steps through the possible values of $\frac{\omega_0}{k}$, the radius runs continuously from zero through infinity and back to zero again, providing a kaleidoscope-like effect. Each slope through the origin of the (ω_0, k) plane provides a different global shape.

To sample over the different types of trajectories possible for $\omega_0 > 0$ and $k > 0$, we first held $\omega_0 = 1$ and varied k from 0 to 1, and then held $k = 1$ and varied ω_0 from 0 to 1, as shown in Figure 3.8. Some example trajectories are shown in Figures 3.9 and 3.10. From simulations, we have found that the global radius goes to approximately infinity when $\frac{\omega_0}{k} = 0.1292 + 0.1189n$, where n is an integer.
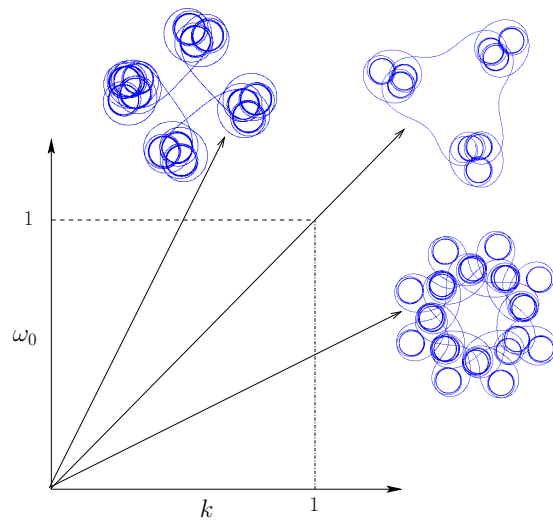
Figure 3.8: The trajectories along each line with slope $\frac{\omega_0}{k}$ vary only in scale. By holding $\omega_0 = 1$ and sampling over $k \in [0, 1]$, as shown by the dashed line, and by holding $k = 1$ and sampling over $\omega_0 \in [0, 1]$, as shown by the dash-dot line, all possible trajectories for $\omega_0 > 0$ and $k > 0$ are sampled.
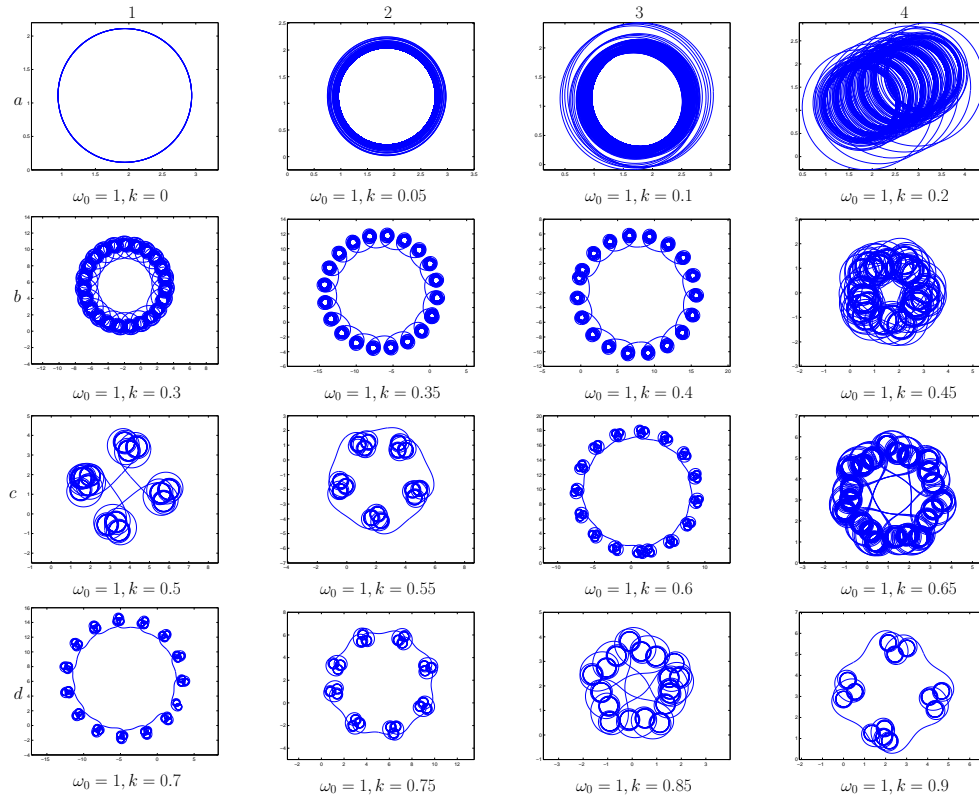
Figure 3.9: A few examples of vehicular trajectories for v_1 from coupling function (2.10) with $\mu_1 = 0.1, \mu_2 = 1$, and $\mu_3 = -0.06$, while holding $\omega_0 = 1$ and varying k from 0 to a value close to 1.
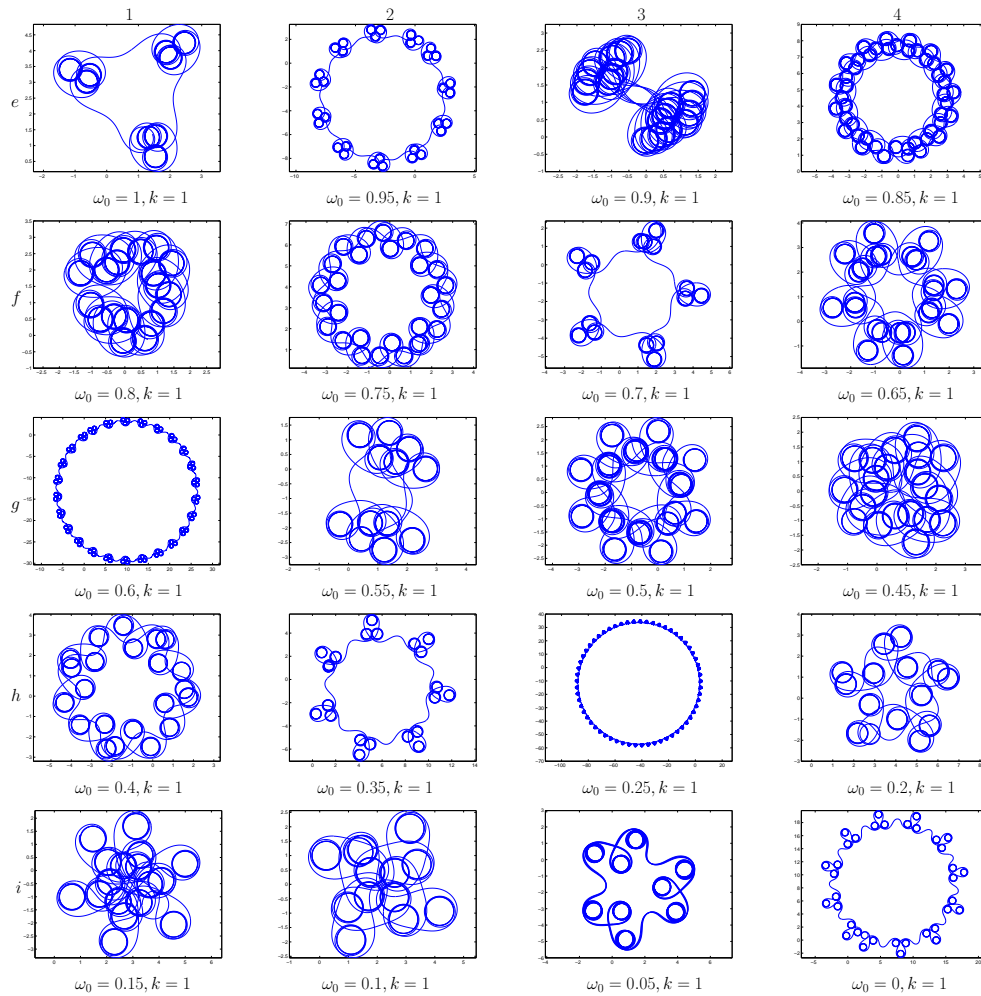
Figure 3.10: A continuation of Figure 3.9: A few example vehicular trajectories for v_1 holding $k = 1$ and varying ω_0 from 1 to 0.

Chapter 4

Results for Heterogeneous

Coupling Topology

We have also found interesting ψ dynamics and vehicular trajectories for coupling topologies other than all-to-all. We assume that all coupling links are weighted equally, and that it is possible to have uni-directional coupling[1], but that there cannot be more than one coupling link in a particular direction between any two oscillators. Given this, there are thirteen different coupling topologies possible for three oscillators. These assumptions are reasonable because we have not included anything in the model that allows each vehicle to weight input unevenly, which would be the case of having two coupling links in the same direction between the same two agents. On a generic level, we have provided a means for categorizing each topology in Figure 4.1, which also shows all-to-all coupling: each link is assigned a

---

[1]The direction of the arrow indicates which oscillator can access the relative information - the oscillator at the point of the arrow has access to the relative information of the oscillator at the back of the arrow.
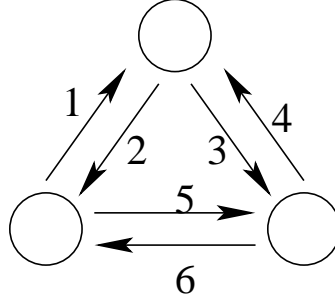
Figure 4.1: The numbering scheme for the topology classification. The shown all-to-all coupling topology is denoted as 123456.

number, and each coupling topology is characterized by the link numbers it has.

Using this numbering scheme, the twelve other topologies are shown in Figure 4.2. Scheme 1234 provides some interesting vehicular trajectories, and will be investigated further in this section. We have nicknamed scheme 1234 the "Arbiter" configuration.

4.1   Results for the Arbiter Configuration

For the Arbiter configuration and the particular coupling function used in the Example in Section 2.3 with $k = 1$, $\mu_1 = 0.1$, $\mu_2 = 1$, and $\mu_3 = -0.06$, we have found a stable periodic orbit in the (ψ_1, ψ_2) coordinates, which indicates that we may find interesting vehicular trajectories. The Arbiter configuration is realistic for the case where the vehicles are almost aligned, with each vehicle spaced far enough apart that the vehicles on the ends of the line cannot sense each other, and therefore must communicate with each other via the vehicle in the center.
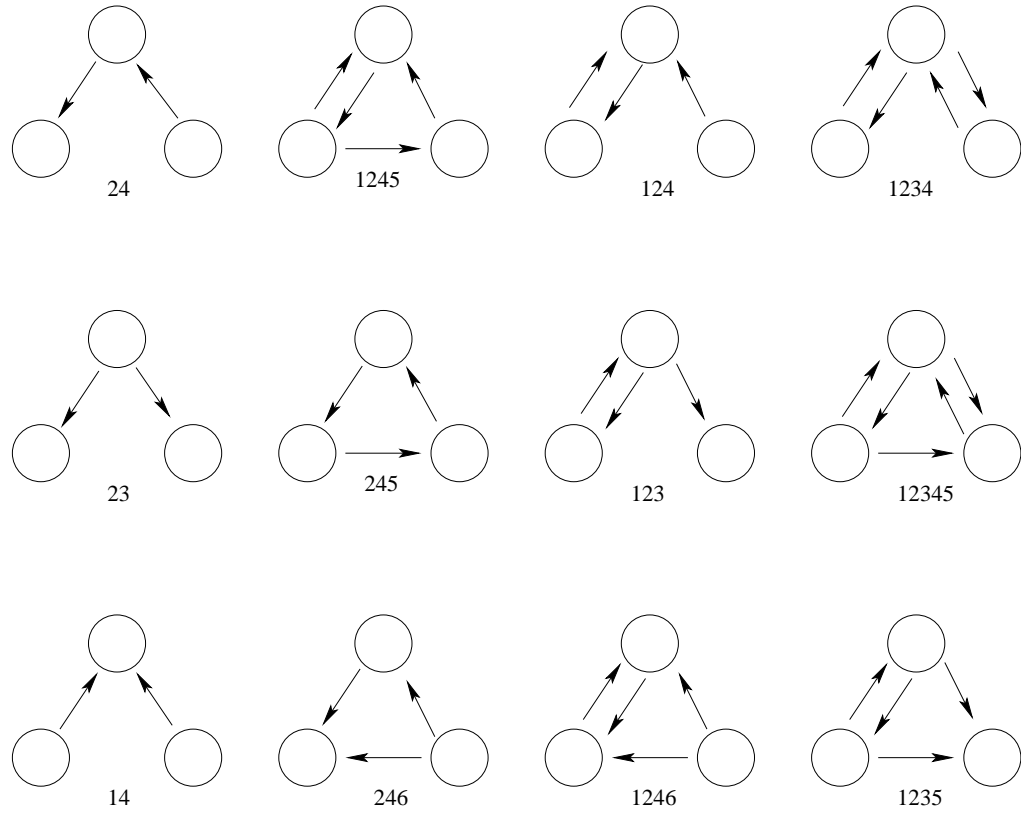
Figure 4.2: Twelve different coupling topologies: we assume that all of the oscillators and coupling links are identical and that there cannot be more than one link between any two oscillators in any direction. Given these constraints, these twelve plus the all-to-all coupling scheme in Figure 4.1 represent all possible coupling topologies.

4.1.1 Solutions

The equations for the Arbiter configuration for $N = 3$ are

$$\dot{\theta}_1 = \omega_0 + k \left(f(\theta_2 - \theta_1) + f(\theta_3 - \theta_1) \right),$$

$$\dot{\theta}_2 = \omega_0 + k f(\theta_1 - \theta_2), \tag{4.1}$$

$$\dot{\theta}_3 = \omega_0 + k f(\theta_1 - \theta_3).$$

Transforming Eqns (4.1) into the ψ coordinates as in Section 2.3 gives

$$\dot{\psi}_1 = k \left(f(-\psi_1) + f(-\psi_2) - f(\psi_1) \right),$$

$$\dot{\psi}_2 = k \left(f(-\psi_1) + f(-\psi_2) - f(\psi_2) \right). \tag{4.2}$$

It is evident that the (ψ_1, ψ_2) equations are equivariant under permutation of ψ_1 and ψ_2, and that the lines $\psi_1 = 2\pi n$ and $\psi_2 = 2\pi n$, where n is an integer, are no longer invariant. The system does have an invariant line at $\psi_1 = \psi_2$. Along this line, $\psi_1 = \psi_2 \equiv \psi$, so we have that if there exists a ψ^* such that $2f(-\psi^*) - f(\psi^*) = 0$, then there will be at least one fixed point on the invariant line. An argument for the existence of such a ψ^* will be given in the $S_2 \times S_1$ fixed point analysis below.

The solutions guaranteed to exist for the all-to-all coupling topology are now subject to some conditions to exist for the Arbiter coupling topology.

The S_3 Solution: Fixed Point at $(\psi_1^*, \psi_2^*) = (0, 0)$

For the S_3 phase-locked solution to exist, we must have that $2f(0) - f(0) = 0$, or, equivalently, that $f(0) = 0$. Should this solution exist, linearization of the ψ equations shows that the fixed point will have eigenvalues $\lambda_1 = -3k f'(0)$ and

$\lambda_2 = -kf'(0)$, so the S_3 solution cannot have complex eigenvalues and will be either a sink or a source if it exists. A bifurcation of this fixed point requires that $f'(0) = 0$.

The Z_3 Solutions: Fixed Points at $(\psi_1^*, \psi_2^*) = (\frac{2\pi}{3}, \frac{4\pi}{3})$ and $(\frac{4\pi}{3}, \frac{2\pi}{3})$

The Z_3 phase-locked solutions require that $f(\frac{4\pi}{3}) = f(\frac{2\pi}{3}) = 0$ to exist. Should this solution exist, the Jacobian of the ψ equations have the eigenvalues $\lambda_{1,2} = -k\left(f'(\frac{2\pi}{3}) + f'(\frac{4\pi}{3}) \pm \sqrt{f'(\frac{2\pi}{3})f'(\frac{4\pi}{3})}\right)$. If $f'(\frac{2\pi}{3})f'(\frac{4\pi}{3}) < 0$ and $-k\left(f'(\frac{2\pi}{3}) + f'(\frac{4\pi}{3})\right) < 0$ (resp., $-k\left(f'(\frac{2\pi}{3}) + f'(\frac{4\pi}{3})\right) > 0$), then this point will be a spiral sink (resp., spiral source). If If $f'(\frac{2\pi}{3})f'(\frac{4\pi}{3}) > 0$, then the point can be either a sink, source, or saddle. If $f'(\frac{2\pi}{3}) + f'(\frac{4\pi}{3}) = 0$, then we would expect a Hopf bifurcation.

The $S_2 \times S_1$ Solution: Fixed Points with $\psi_1 = \psi_2$

The condition for the existence of the existence of the $S_2 \times S_1$ solution is that there exists a δ^* such that $2f(-\delta^*) - f(\delta^*) = 0$. As noted earlier, this is the same condition for the existence of a fixed point on the invariant line $\psi_1 = \psi_2 \equiv \psi$. As before, we will assign two new functions, $c_1(\delta) = 2f(-\delta)$ and $c_2(\delta) = f(\delta)$, and a valid δ^* will satisfy

$$c_1(\delta^*) = c_2(\delta^*). \tag{4.3}$$

If $|f(\delta)| > 0$ for all δ, then this solution is not guaranteed to exist, since it is

then possible to have $|c_1(\delta) - c_2(\delta)| > 0$ for all δ, implying that Eqn (4.3) may not be satisfied for any δ. Therefore, we assume that there exists a ϕ_1 such that $f(\phi_1) = 0$, but $f'(\phi_1) \neq 0$. Then, by periodicity of f, there must be some ϕ_2 such that $f'(\phi_2) = 0$ but $f'(\phi_2) \neq 0$. We will also assume that the S_3 solution does not exist (i.e., $\delta^*, \phi_1, \phi_2 \neq 0$). Then we have that $f(\theta)$, for $\theta \in [0, 2\pi)$, will have both positive and negative values. As before, the definitions of $c_1(\delta)$ and $c_2(\delta)$ give that $c_1(0) = 2c_2(0)$, but $c_1'(0) = -2c_2'(0)$. Given these constraints, we expect to have one of the two situations shown in Figure 4.3. In both situations, we expect to find an even number of $S_2 \times S_1$ solutions provided $f'(\delta_j^*) \neq 0$ for all $j \in \mathbb{Z} > 0$.

Without loss of generality, we will assume that $c_1(0) > c_2(0) > 0$. This implies that $c_1(2\pi) > c_2(\pi) > 0$. Then, by the periodicity of f, we have that

$$\min c_2(\delta) = \min f(\delta) \equiv \beta,$$

$$\min c_1(\delta) = \min(2f(-\delta)) = \min(2f(\delta)) = 2\min f(\delta) = 2\beta,$$

where $\beta < 0$. This is shown clearly in Figure 4.4. This implies that there exists a δ^{**} such that $c_1(\delta^{**}) < c_2(\delta^{**})$. Therefore, by the intermediate value theorem, we have that there must be at least two valid values $\delta_{1,2}^*$ such that $c_1(\delta_1^*) = c_2(\delta_1^*)$ and $c_1(\delta_2^*) = c_2(\delta_2^*)$. Furthermore, all further viable values for δ_{2j+1}^*, for $j \in \mathbb{Z} \geq 1$, must be accompanied by a viable value for δ_{2j+2}^*; that is, δ^*s will occur in pairs.

If the S_3 solution exists but the other conditions hold, one can apply the previous argument to show that there will still be an even number of intersections; however, one of those intersections will be the degenerate case where $\delta^* = 0$. That solution will not be a general $S_2 \times S_1$ solution; that is the S_3 solution. Because of this, we
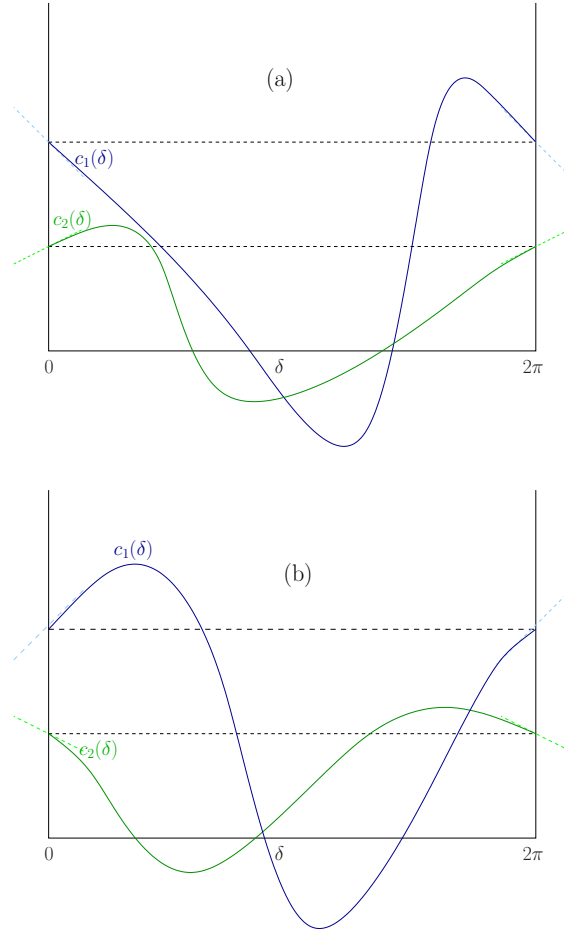
Figure 4.3: Illustration of the two possible scenarios used in the argument for the existence of the $S_2 \times S_1$ phase-locked solution for the Arbiter coupling topology with a general 2π-periodic coupling function f. Here we assume that the S_3 solution does not exist, and that there exists a ϕ_1 such that $f(\phi_1) = 0$ but $f'(\phi_1) \neq 0$. In (a), we show the case where $c_1'(0) < 0$, and in (b), the case where $c_1'(0) > 0$. The light blue lines show $c_1'(0) = c_1'(2\pi)$ and the light green lines show $c_2'(0) = c_2'(2\pi)$.
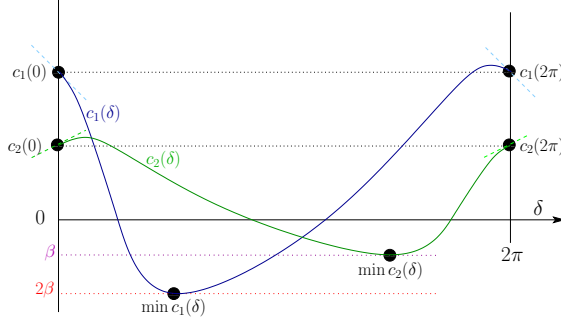
Figure 4.4: Illustration of the argument that given the constraints mentioned in the text, that there must be at least two possible values for δ^*. Without loss of generality, we can set $c_1(0) > c_2(0) > 0$, which gives $c_1(2\pi) > c_2(2\pi) > 0$ by periodicity. However, by noting that min $f(-\delta) = \min f(\delta)$, it is obvious that $\min c_1(\delta) = 2 \min c_2(\delta)$. Therefore, $c_1(\delta)$ and $c_2(\delta)$ must cross at a minimum of two points. The points where the two functions cross are viable values for δ^*, and proves the existence of the $S_2 \times S_1$ solution.

expect an odd number of $S_2 \times S_1$ solutions should the S_3 solution exist, but that there will be at least one viable value for δ^* given the conditions mentioned above.

4.1.2 Application to the Particular Example

Using the example coupling function (2.10) with $\mu_1 = 0.1$, $\mu_2 = 1$, $\mu_3 = -0.06$, and $k = 1$, it is possible to solve for the exact fixed points of the system for the parameters given. This particular system has saddle points at $(\psi_1^*, \psi_2^*) = (4.29213, 4.29213)$ and $(1.35235, 1.35235)$, and spiral sinks at $(\psi_1^*, \psi_2^*) = (4.8432, 1.63105)$ and $(1.63105, 4.8432)$. These are shown in Figure 4.5.

The motion from the coupling function (2.10) with this communication topology also produces interesting trajectories, reminiscent of those found in Section 2.3. The ψ plane for $N = 3$ in Figure 4.5 has the corresponding vehicular motion shown in Figure 4.6. For the same reasons as in Section 3.2.4, one can also produce a variety of trajectories by varying the values of ω_0 and k, as shown in Figure 4.7.
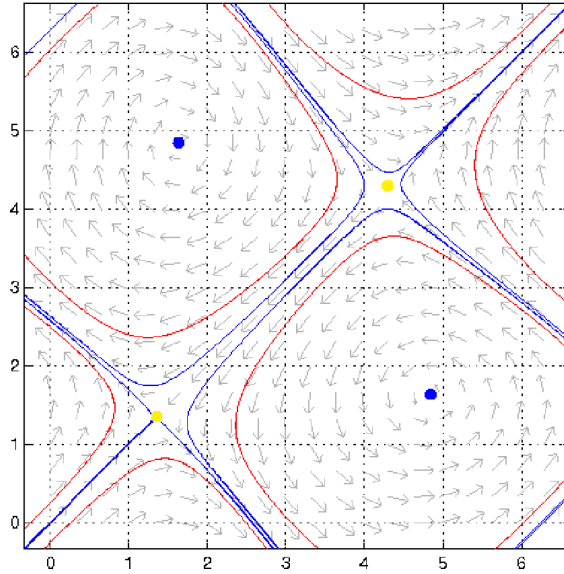
Figure 4.5: The (ψ_1, ψ_2) plane for the Arbiter coupling topology with $N = 3$, and coupling function (2.10) with $\mu_1 = 0.1, \mu_2 = 1, \mu_3 = -0.06, \omega_0 = 1, k = 1$. The existence of a stable periodic orbit suggests that this system may provide interesting patterns of vehicular motion.
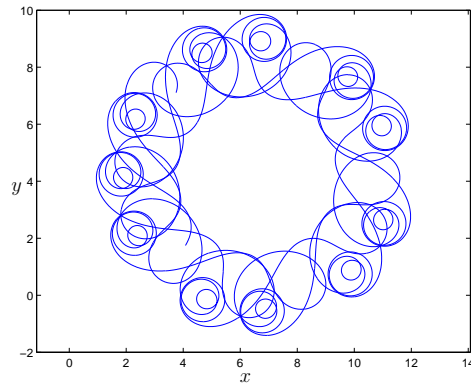
Figure 4.6: Motion of v_1 using the Arbiter coupling topology with $N = 3$ corresponding to the motion of the system along the stable periodic orbit in Figure 4.5.
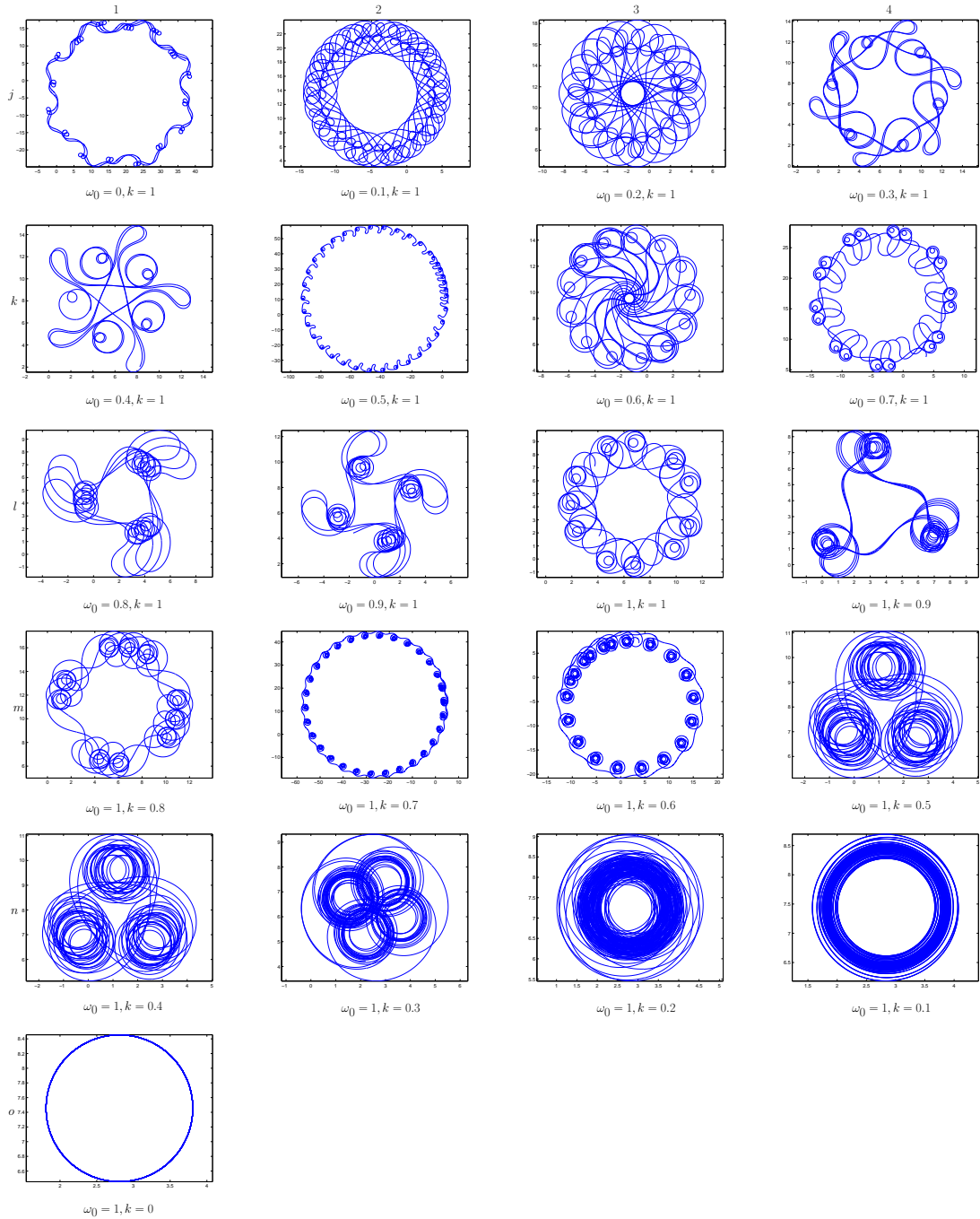
Figure 4.7: Various vehicular trajectories generated using the Arbiter coupling topology and the example coupling function (2.10) with $\mu_1 = 0.1$, $\mu_2 = 1$, $\mu_3 = -0.06$, while varying the values of ω_0 and k, as was done in Figures 3.9 and 3.10.
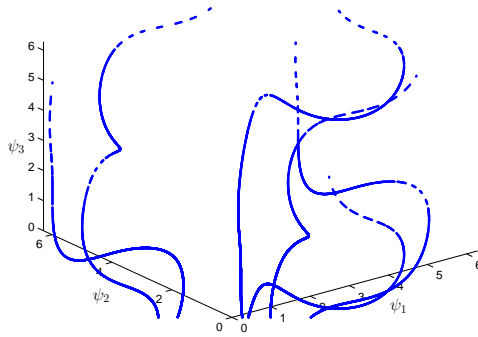
Figure 4.8: The (ψ_1, ψ_2, ψ_3) space for the Arbiter coupling topology and the example coupling function (2.10) with $\mu_1 = 0.1$, $\mu_2 = 1$, $\mu_3 = -0.06$, $\omega_0 = 1$, and $k = 1$. Here ψ_1 and ψ_2 are defined as for $N = 3$, and $\psi_3 \equiv \theta_1 - \theta_4$. As in the $N = 3$ case, the system has a stable periodic orbit.

This periodic orbit also persists for the coupling function (2.10) and the Arbiter configuration with $N = 4$, as shown in Figure 4.8, which produces the corresponding vehicular motion in Figure 4.9.

Bifurcations

A cartoon of the bifurcations for this system is shown in Figure 4.10. As μ_1 decreases from about 0.2, a pair of periodic orbits is born in a saddle-node bifurcation of periodic orbits, and then the stable periodic orbit terminates in a homoclinic bifurcation. Due to symmetry, there are two pairs of periodic orbits in the (ψ_1, ψ_2) plane. In the bifurcation diagram for the periodic orbits, as μ_1 continues to decrease, the stable periodic orbit is reborn in a homoclinic bifurcation, and eventually the two periodic orbits terminate in a saddle-node of periodic orbits. Numerical bifurcation analysis of the fixed points shows that the saddle point involved in the homoclinic bifurcation undergoes pitchfork bifurcation and that the three fixed
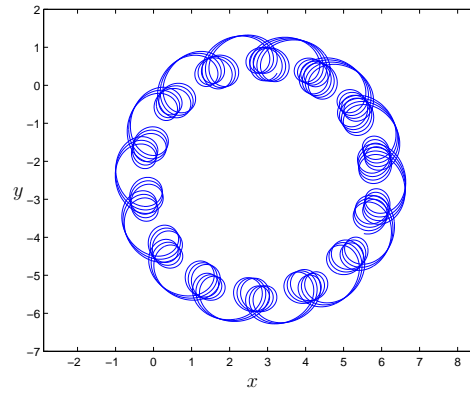
Figure 4.9: Motion of v_1 using the Arbiter coupling topology for $N = 4$ corresponding to the motion of the system along the stable periodic orbit in Figure 4.8.

points depicted below the periodic orbits come together via a pitchfork bifurcation, as μ_1 either increases or decreases past the limits of the periodic orbits, as shown in Figure 4.10.
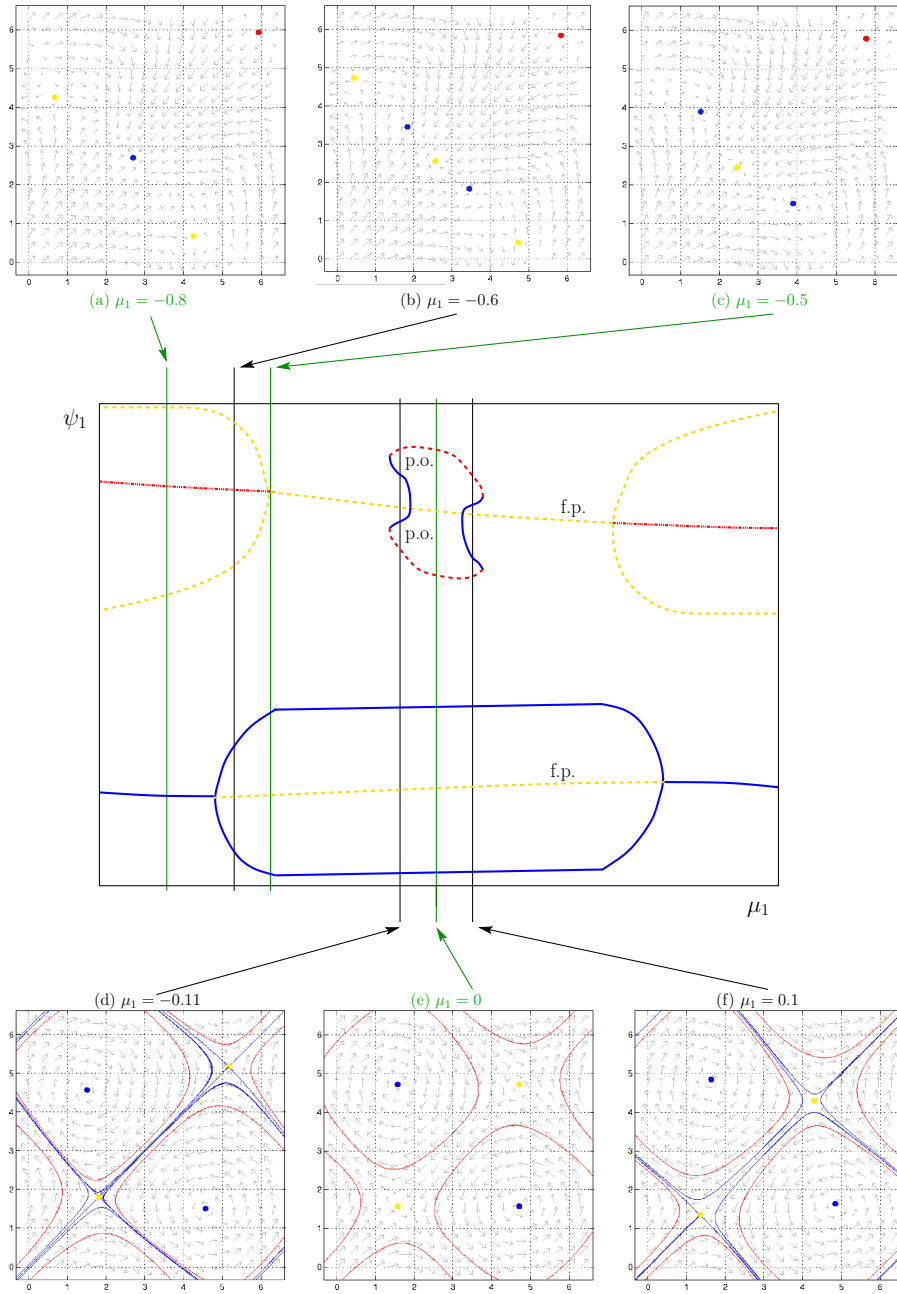
Figure 4.10: A cartoon of the bifurcation diagram for the Arbiter communication topology and the example coupling function (2.10) in terms of the parameter μ_1. In both the bifurcation diagram and in the phase portraits, sources are colored red, sinks are blue, and saddle points are yellow. Unstable periodic orbits are shown in red, and stable periodic orbits are shown in blue.

Chapter 5

Conclusion

We have provided a brief explanation of the LPS model, with relevant background information from related fields. Our work focuses on a variant of the LPS model, which produces novel vehicular trajectories. Since the results of the LPS model can be analyzed in terms of the solutions to a simplified Kuramoto equation, we have provided an analysis of our phase controller, with our modified coupling function, for three vehicles. We have shown a simple way to reduce the order of the phase system by one. Therefore, limiting our system to three vehicles allows us to invoke the Poincare-Bendixson Theorem and limit the solutions of the reduced phase system to periodic orbits and fixed points. While this is a very simple solution in the reduced phase system, it corresponds to exotic vehicular trajectories. In addition to illustrating the range of possible vehicular trajectories, we have developed an intuitive way to relate motion of the system in the reduced ψ coordinates to motion of the vehicles in the plane, and shown that interesting behavior can be

found for coupling topologies other than all-to-all.

The trajectories shown in the previous section may have applications in sensor area covering problems in which one is particularly interested in certain parts of the plane, with the option of either passing through the center or moving along the circumference of the area to be covered. For example, the trajectory shown in 1c of Figure 3.9 may be useful for the case where one wants agents to carefully patrol four evenly distributed areas as well as check the area in the center of those four areas periodically. If one desires to check sections of a circular area but is not interested in the area in the center of the sections, a trajectory such as 2e of Figure 3.10 may be appropriate. Should the areas inside the circular area be of higher interest than the perimeter, then a trajectory such as 2n of Figure 4.7 may be of interest. If one desires to patrol an annulus, a trajectory similar to 4e of Figure 3.10 may be useful. If a faster but less detailed check of perimeter areas are needed, then a trajectory shape closer to the one shown in Figure 4.9 may be more appropriate.

The trajectories found here are quite sensitive to uncertainty in the parameters of the coupling equations. Should these trajectories prove to be potentially useful for a particular area coverage problem, it may be worthwhile to work through the spacing control, and to make the global behavior robust to perturbations in the parameters. The trajectories found and the explanation of what causes these interesting group motions also provides insight on how to shape the trajectories of vehicles by controlling the features of the (ψ_1, ψ_2) plane, as well as how this type of system may be extended to the more general case, where $N > 3$.

Bibliography

[1] Spirograph. http://en.wikipedia.org/wiki/Spirograph. A short history on the Spirograph.

[2] P. Ashwin, O. Burlko, P. Maistrenko, and O. Popvych. Extreme sensitivity to detuning for globally coupled phase oscillators. *Physical Review Letters*, 96(054102), 2006.

[3] P. Ashwin, G. King, and J. Swift. Three identical oscillators with symmetric coupling. *Nonlinearity*, 3:585–601, 1990.

[4] P. Ashwin and J. Swift. The dynamics of n weakly coupled identical oscillators. *Journal of Nonlinear Science*, 2:69–108, 1992.

[5] E. Brown, P. Holmes, and J. Moehlis. Globally coupled oscillator networks. In E. Kaplan, J. Marsden, and K. Sreenivasan, editors, *Perspectives and Problems in Nonlinear Science: A Celebratory Volume in Honor of Larry Sirovich*, pages 183–215. Springer, 2003.

[6] L. Dubins. On curves of minimal length with a constraint on average curvature,

and with prescribed initial and terminal positions and tangents. *American Journal of Mathematics*, 79(3):497–516, 1957.

[7] A. Garg. Spirograph: spirographs. http://wordsmith.org/~anu/java/spirograph.html. An interactive applet on spirograph patterns.

[8] D. Hansel, G. Mato, and C. Meunier. Clustering and slow switching in globally coupled phase oscillators. *Physical Review E*, 48(5):3470–3477, 1993.

[9] E. Justh and P. Krishnaprasad. A simple control law for uav formation flying. Technical report, Institute for Systems Research, 2002.

[10] A. Kolpas and J. Moehlis. Optimal switching between coexisting stable collective motion states. Submitted.

[11] Y. Kuramoto. Lecture notes in physics. In H. Arakai, editor, *International Symposium on Mathematical Problems in Theoretical Physics*. Springer, 1975.

[12] B. Nabet, N. Leonard, I. Couzin, and S. Levin. Leadership in animal group motion: A bifurcation analysis. In *Proc. 17th Int. Symp. on Mathematical Theory of Networks and Systems*, 2006.

[13] D. Paley, N. Leonard, and R. Sepulchre. Collective motion: Bistability and trajectory tracking. In *Proc. 43rd IEEE Conf. Decision and Control*, pages 1932–1937, 2004.

[14] D. Paley, N. Leonard, and R. Sepulchre. Oscillator models and collective

motion: Splay state stabilization of self-propelled particles. In *Proc. 44th IEEE Conf. Decision and Control*, 2005.

[15] D. Paley, N. Leonard, R. Sepulchre, and D. Grunbaum. Oscillator models and collective motion. Submitted.

[16] A. Pikovsky, M. Rosenblum, and J. Kurths. *Synchronization: A universal concept in nonlinear sciences*. Cambridge Nonlinear Science Series 12. Cambridge University Press, New York, 2001.

[17] R. Sepulchre, D. Paley, and N. Leonard. Collective motion and oscillator synchronization. In V. Kumar, N. Leonard, and A. Morse, editors, *Proc. 2003 Block Island Workshop on Cooperative Control*, pages 1–17. Springer-Verlag, 2003.

[18] R. Sepulchre, D. Paley, and N. Leonard. Graph Laplacian and Lyapunov design of collective planar motions. In *Proc. NOLTA*, 2005.

[19] R. Sepulchre, D. Paley, and N. Leonard. Stabilization of planar collective motion part I: All-to-all communication. *IEEE Transactions on Automatic Control*, 52(5):811–824, 2007.

[20] I. Stewart, M. Golubitsky, and M. Pivato. Symmetry groupoids and patterns of synchrony in coupled cell networks. *SIAM J. Applied Dynamical Systems*, 2(4):609–646, 2003.

[21] S. Strogatz. From Kuramoto to Crawford: exploring the onset of synchronization in populations of coupled oscillators. *Physica D*, 143:1–20, 2000.

[22] H. Sussmann. The Markov-Dubins problem with angular acceleration control. In *Proc. 36th IEEE Conference on Decision and Control*, pages 2639–2643, 1997.

[23] A. Winfree. Biological rhythms and behavior of populations of coupled oscillators. *J. Theoretical Biology*, 16:15, 1967.